NASA TECHNICAL NOTE

NASA TN D-6454

EFFECT OF VELOCITY PROFILE DISTORTION IN CIRCULAR TRANSVERSE-FIELD ELECTROMAGNETIC FLOWMETERS

by Norman C. Wenger

Lewis Research Center
Cleveland, Ohio 44135

NATIONAL AERONAUTICS AND SPACE ADMINISTRATION • WASHINGTON, D. C. • AUGUST 1971

1. Report No.	2. Government Accession No.	3. Recip..
NASA TN D-6454		

4. Title and Subtitle	5. Report Date
EFFECT OF VELOCITY PROFILE DISTORTION IN CIRCULAR TRANSVERSE-FIELD ELECTROMAGNETIC FLOWMETERS	August 1971
	6. Performing Organization Code
7. Author(s)	8. Performing Organization Report No.
Norman C. Wenger	E-6142
	10. Work Unit No.
9. Performing Organization Name and Address	120-27
Lewis Research Center National Aeronautics and Space Administration Cleveland, Ohio 44135	11. Contract or Grant No.
	13. Type of Report and Period Covered
12. Sponsoring Agency Name and Address	Technical Note
National Aeronautics and Space Administration Washington, D. C. 20546	14. Sponsoring Agency Code

15. Supplementary Notes

16. Abstract

The theory of circular transverse-field electromagnetic flowmeters is extended to include the effect of distortion from axial symmetry in the fluid velocity profile. A general formulation is developed for computing the flowmeter sensitivity for any given velocity profile. It is shown how to best select the flowmeter pipe wall thickness and electrical conductivity to minimize error in the flow measurement due to uncertainties in the velocity profile. The "fully developed" velocity profile and corresponding flowmeter sensitivity are then computed for a Hartmann number range from 1 to 1000. Numerical results are presented in tabular form for a range of flowmeter parameters that is normally found in liquid metal applications. These results enable the experimenter to correct flow measurements for the effect of velocity profile distortion produced by the flowmeter itself.

17. Key Words (Suggested by Author(s))	18. Distribution Statement
Flowmeters; Electromagnetic flowmeters; Flow measurement; Liquid metals; Magnetohydrodynamics; Velocity profiles; Velocity profile distortion; Flow distribution; Velocity distribution; Flow distortion; Magnetohydrodynamic flow	Unclassified - unlimited

19. Security Classif. (of this report)	20. Security Classif. (of this page)	21. No. of Pages	22. Price*
Unclassified	Unclassified	73	$3.00

*For sale by the National Technical Information Service, Springfield, Virginia 22151

CONTENTS

Page

SUMMARY 1

INTRODUCTION 1

THE MODEL - BASIC EQUATIONS AND BOUNDARY CONDITIONS 5
- Preliminary Considerations 5
- The Model 7
- Basic Equations and Boundary Conditions 8

INDUCED POTENTIAL FOR AN ARBITRARY VELOCITY PROFILE 15
- Induced Potential 15
- Flowmeter Sensitivity 17

INDUCED POTENTIAL FOR FULLY DEVELOPED VELOCITY PROFILE 22
- Exact Series Solution 23
  - Solution of basic equations 23
  - Average velocity and induced potential 27
  - Asymptotic solution for small M 28
  - Numerical results for exact series solution 30
- Approximate Solution Using Variational Principle and Ritz Technique 32
  - Variational principle 32
  - Ritz technique 34
  - Evaluation of solution 36
  - Numerical results 39
  - Accuracy of results 43

CONCLUDING REMARKS 48

APPENDIXES
- A - SYMBOLS 49
- B - FLOWMETER PARAMETERS 52

REFERENCES 54

EFFECT OF VELOCITY PROFILE DISTORTION IN CIRCULAR TRANSVERSE-FIELD ELECTROMAGNETIC FLOWMETERS

by Norman C. Wenger

Lewis Research Center

SUMMARY

The theory of circular transverse-field electromagnetic flowmeters is extended to include the effect of distortion from axial symmetry in the fluid velocity profile. A general formulation is developed for computing the flowmeter sensitivity for any given velocity profile. It is shown how to best select the flowmeter pipe wall thickness and electrical conductivity to minimize error in the flow measurement due to uncertainties in the velocity profile. The "fully developed" velocity profile and corresponding flowmeter sensitivity are then computed for a Hartmann number range from 1 to 1000. Numerical results are presented in tabular form for a range of flowmeter parameters that is normally found in liquid metal applications. These results enable the experimenter to correct flow measurements for the effect of velocity profile distortion produced by the flowmeter itself.

INTRODUCTION

Electromagnetic flowmeters have been used for many years to measure the flow rates of a great variety of electrically conductive fluids including blood. The advent of nuclear reactors and associated energy conversion devices that use liquid metal coolants has caused renewed interest in electromagnetic flowmeters.

Electromagnetic flowmeters use Faraday's law as the basic principle of operation. The motion of a fluid through a stationary magnetic field induces a potential gradient in the fluid. The value of this potential gradient, which is indicative of the flow rate, can be determined by measuring the potential difference between electrodes which are in electrical contact with the fluid. If the fluid has a high electrical conductivity, the potential gradient will result in a large induced current in the fluid. The induced current produces a magnetic field which can also be measured and used to indicate the flow rate. Flow-

meters which use this latter principle are generally referred to as induced-field flowmeters.

Although there are many types of electromagnetic flowmeters in use, the most common type for liquid metal applications and the only type that will be considered in this report is the transverse-field flowmeter shown in figure 1. The flow is contained in a circular pipe which is normally made from nonmagnetic materials such as 316 stainless steel. A permanent magnet or direct current electromagnet is used to produce the uni-

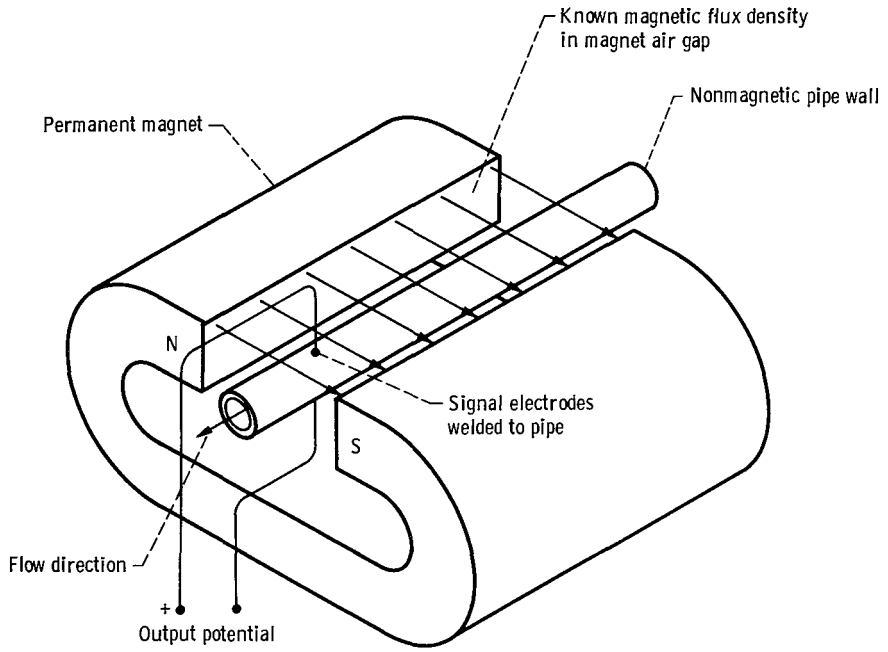

Figure 1. - Transverse-field electromagnetic flowmeter.

form transverse static magnetic field. Electrodes for detecting the induced potential are located on a pipe diameter which is perpendicular to both the pipe axis and magnetic field. If the pipe wall is conductive, which is the most common situation found in practice, the electrodes are fastened to the outer wall of the pipe as shown. If the pipe wall is nonconductive, however, the electrodes must penetrate the wall to be in electrical contact with the fluid.

There are several reasons for the popularity of this type of flowmeter. In addition to its basic simplicity, it does not require that the pipe be cut open during installation if the pipe wall is conductive since nothing is inserted directly into the flow stream. This is particularly advantageous in applications involving corrosive liquid metals where the

opening of a line to insert a flowmeter is both a possible source of contamination to the liquid metal and a hazard to the personnel involved.

The main problem with this and all other types of electromagnetic flowmeters is determining the relation between the measured potential and the average fluid velocity or flow rate. Early studies of this problem by Williams (ref. 1), Thürlemann (ref. 2), and Kolin (ref. 3) considered the case where the pipe wall was nonconductive and where the fluid velocity profile was symmetric about the axis of the pipe. It was found that the output potential is simply equal to the product of the pipe inner diameter, the applied transverse magnetic flux density, and the average fluid velocity. This result is valid for any velocity profile as long as the profile has axial symmetry.

Several years later, Elrod and Fouse (ref. 4) considered the case where the pipe wall is conductive. They found that the output potential for this case is also proportional to the average fluid velocity as long as the velocity profile has axial symmetry. For the same flow rate, the output potential is reduced from that found for a nonconducting pipe by a factor which involves the fluid and wall conductivity and the wall thickness.

In many cases found in practice, the velocity profile of the fluid is not axially symmetric. This asymmetry can be due to two effects. If the flowmeter were located immediately downstream from an elbow or obstruction in the flowline, the velocity profile can be greatly distorted from axial symmetry. The obvious solution of moving the flowmeter further downstream may not be possible in many cases. The second cause of velocity profile distortion from axial symmetry is the flowmeter itself. If the fluid is highly conductive, as in the case of liquid metals, the large induced current interacts with the applied magnetic field and produces a force on the fluid. This force, which is nonsymmetrical, is normally quite large and severely distorts the velocity profile from axial symmetry. This distortion can be reduced by decreasing the intensity of the applied magnetic field. However, the output potential, which is approximately proportional to the applied magnetic field intensity, will normally vanish into the ambient electrical noise before the distortion becomes negligible.

Considerable effort has been expended to determine how the velocity profile affects the output potential and, hence, the measurement of the average fluid velocity. A general formulation has been developed by Shercliff (refs. 5 and 6) showing the relation between the output potential and the velocity profile. This formulation is valid for any velocity profile, but it is limited to the case where the pipe wall is nonconductive. In the first part of this report, this formulation is extended to the case where the pipe wall is conductive. This formulation allows the experimenter who has some knowledge of the general shape of the velocity profile to compute a more accurate relation between the output potential and the average fluid velocity. It also shows how to best select the pipe wall thickness and conductivity to minimize the effect of uncertainties in the velocity profile. This formulation is most applicable when the fluid is a poor conductor so that the velocity profile in the flowmeter depends on conditions upstream from the flowmeter and may be predictable.

In the second part of this report, the effect of self-induced velocity profile distortion by the flowmeter itself is considered in detail. The exact solution for the velocity profile has been obtained by Ufland (ref. 7), Uhlenbusch and Fischer (ref. 8), and Gold (ref. 9) for the case where the pipe wall is nonconductive. The solutions are in the form of an infinite series involving modified Bessel functions of the first kind. The significant figure requirement for summing these series exceeds that of modern computers, however, unless the Hartmann number M, which is the ratio of the electromagnetic forces to the viscous forces in the fluid, is less than about 20. The range of Hartmann numbers encountered in liquid metal applications is typically 50 to 500.

An asymptotic solution for the velocity profile at large Hartmann numbers has been obtained by Singh and Noriboli (ref. 10) for the nonconductive pipe wall case. Although their results seem reasonable, their solution cannot be formally justified. The Bessel functions in the series solution were replaced by an asymptotic form valid only when the argument, which is large but finite, is much larger than the order of the Bessel functions. The series was summed, however, from order zero to infinity (ref. 9).

Some work has been done on the conductive pipe wall case when the wall has finite thickness. Shercliff (ref. 11) obtained a solution for the velocity profile and induced output potential using an iterative technique. These solutions are in the form of power series in the Hartmann number up to the term M^2. The series give useful numerical values for the velocity profile and output potential only for M less than 2.

Considerable work has been done on the conducting pipe wall case using the "thin wall" approximation. In this approximation, the pipe wall is assumed to be sufficiently thin so that the effect of the wall can be incorporated into a boundary condition at the pipe inner radius. Using this approximation, Ihara, Tajima, and Matsushima (ref. 12) obtained a solution in infinite series form which also suffered from the same numerical difficulties as did previous nonconductive wall solutions for Hartmann numbers greater than about 20. Also using the thin wall approximation, Shercliff (refs. 11 and 13), Chang and Lundgren (ref. 14), and Gold (ref. 15) obtained approximate asymptotic solutions at large M for the velocity profile and average fluid velocity. These solutions do not account fully for the effect of the boundary layer at the pipe wall. Moreover, only Shercliff (refs. 11 and 13) computed the output potential. The output potential solution is approximate and holds only over a limited range of Hartmann number and pipe wall conductivity.

This report presents a solution for the output potential as a function of the average velocity for the fully developed velocity profile. The pipe wall is assumed to be conductive and of arbitrary thickness. The solution is obtained using a variational principle for magnetohydrodynamic channel flow (refs. 16 and 17) and the Ritz approximation technique.

The problem is also solved exactly using a procedure similar to that used in references 7 to 10 and 12. The exact solution, which is in infinite series form, also suffers

from numerical difficulties at large M. It is useful, however, at low M for testing the variational solution which is approximate.

Sufficient numerical results from the variational solution are presented so that the experimenter, by interpolating between the computed points, can obtain accurate values for correcting measurements for the effect of velocity profile distortion due to the flowmeter itself. The parameter values covered are as follows: Hartmann number - 1, 2, 5, 10, 20, 50, 100, 200, 500, and 1000; ratio of pipe wall to fluid conductivity - 0, .1, .5, 1., 1.5, and 2.; and ratio of outer-to-inner pipe diameter - 1., 1.05, 1.15, 1.25, and 1.35.

THE MODEL - BASIC EQUATIONS AND BOUNDARY CONDITIONS

Preliminary Considerations

The motion of a conducting fluid through an electromagnetic flowmeter is a complex process. The velocity profile of the fluid at the entrance to the flowmeter is determined by conditions upstream from the flowmeter. As the fluid approaches the magnetic field region, electric currents are induced in the fluid which react with the applied magnetic field and produce a force on the fluid. If the fluid is a poor conductor or the magnetic field is weak (i.e., low Hartman number), this force is small and the fluid velocity profile remains essentially unchanged when passing through the flowmeter. However, if the Hartmann number is large, the velocity profile changes significantly with distance and time as the fluid travels through the magnetic field region. If the applied transverse magnetic field is uniform along the pipe axis and of sufficient extent, the velocity profile will eventually reach an equilibrium profile or "fully developed" profile. From this point on the profile does not change with distance or time until the fluid nears the downstream end of the magnetic field region. After the fluid exits the flowmeter, the velocity profile eventually relaxes to axial symmetry barring any obstruction or elbow in the line.

The ideal point to connect the electrodes for measuring the induced potential is after the velocity profile is fully developed. This choice has several advantages. If the electrodes were located at a point further upstream, the analysis becomes very difficult since the velocity profile at that point is dependent on upstream conditions which may be unknown. Furthermore, in this entrance region the induced potential varies with distance along the pipe. Consequently, the output potential depends not only on the velocity profile in the plane where the electrodes are attached but also on the velocity profile at points upstream and downstream as well. Any analysis of this region must, of necessity, be three-dimensional. In the fully developed region, however, there are no variations with respect to distance along the pipe so that a two-dimensional analysis is adequate.

Another factor that must be considered is whether the flow is turbulent or nonturbulent. Many, if not most, flows in liquid metal practice are turbulent. It has been found experimentally, however, that the imposition of a magnetic field transverse to the flow will suppress turbulence and raise the critical Reynolds number from about 2000 to a substantially higher value. If the magnetic field strength is sufficiently high, the flow in the fully developed region can be made nonturbulent. This provides a great simplification in the analysis since the time varying terms in the fluid dynamic equations need not be considered.

Thus, to apply the results of this analysis it is necessary to know the required distance or entry length to achieve a fully developed profile for proper selection of the magnet dimensions and electrode placement. And it is necessary to determine the critical Reynolds number to ensure nonturbulent flow.

The required entry length has been considered both theoretically and experimentally by Shercliff (refs. 6, 13, and 18) for the nonconductive pipe wall case. By using a Rayleigh type of approximation, Shercliff found that for nonturbulent flow the entry length L is of the order of

$$L \approx Re \frac{a}{M} \tag{1}$$

where Re is the Reynolds number, a the pipe inner radius, and M the Hartmann number which is assumed to be large. Using $Re = 10^4$ and $M = 10^2$, which are typical values found in practice, results in an entry length of 100 pipe radii. Experimental values for the entry length (ref. 13) are generally about one-half those given by equation (1). For the case of a conductive pipe wall the computed entry length is reduced by the factor $1/\gamma M(R - 1)$ (ref. 6) giving

$$L \approx Re \frac{a}{\gamma M^2 (R - 1)} \tag{2}$$

where γ is the ratio of the wall to fluid conductivity and R the ratio of the pipe outer-to-inner radii. Equation (2) is based on the assumption that $\gamma M(R - 1) \gg 1$. For the same values of Re and M used previously, the predicted entry length is 5 pipe radii for $R = 1.2$ and $\gamma = 1$. An experimental investigation of the entry length has not been made for the conducting wall case nor has the problem of a turbulent entry flow been considered for either case. These should be worthwhile areas to explore in future investigations.

The required magnetic field strength necessary to suppress turbulence has received considerable attention, however. The experimental work of Shercliff (ref. 6) and

Loeffler, Maciulaitis, and Hoff (ref. 19) has indicated that the critical Reynolds number Re_{crit} for a circular pipe with a nonconductive wall is given by

$$Re_{crit} = 250\ M \tag{3}$$

for large M. No results are available on the critical Reynolds number for the conducting pipe wall case. However, it is expected that the increased electric current in the fluid which results when the pipe wall is conductive will give greater stability to the flow and increase the critical Reynolds number from that given by equation (3). Experimental verification of this effect is also a worthwhile area for future investigations.

Thus, to use the results based on the velocity profile in the fully developed region, it is necessary that the magnetic field be at least a few entry lengths in extent along the pipe axis and that the electrodes be attached at least an entry length from the upstream end of the flowmeter. Furthermore, the magnetic field strength should be sufficiently large so that the Reynolds number is less than the critical Reynolds number to ensure nonturbulent flow.

The Model

The model to be analyzed is shown in figure 2. The pipe has inner radius a and outer radius b and its axis coincides with the z-coordinate axis. The flow is in the positive z-direction. The magnetic permeability of the pipe wall is assumed to equal that of free-space. The applied magnetic field $\vec{B}_o$ is uniform (independent of x, y, and z) and is alined parallel to the x-axis. If the pipe wall is conductive, the induced output poten-

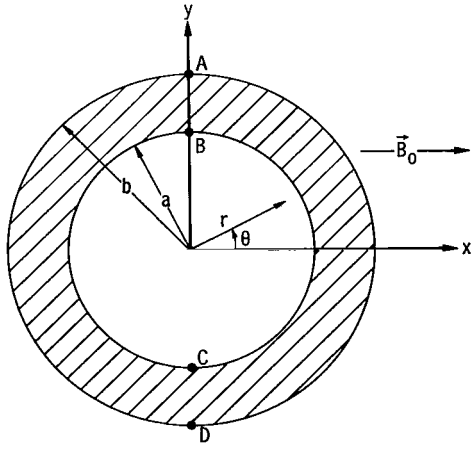

Figure 2. - Pipe cross section.

tial is measured between points A and D. If the pipe wall is nonconductive, the potential is measured between points B and C. In all cases it is assumed that the electrodes draw no current from the flowmeter and that the region beyond the pipe outer radius is an insulator.

Basic Equations and Boundary Conditions

The basic equations to be used are the standard magnetohydrodynamic equations for steady state, fully developed, incompressible, nonturbulent flow. These equations, which consist of Maxwell's equations, the continuity equation, the momentum transport equation, and the generalized Ohm's law, are given by

$$\nabla \times \vec{E} = \vec{0} \tag{4a}$$

$$\nabla \times \vec{B} = \mu_o \vec{J} \tag{4b}$$

$$\nabla \cdot \vec{B} = 0 \tag{4c}$$

$$\nabla \cdot \vec{E} = \frac{\rho_e}{\epsilon_o} \tag{4d}$$

$$\nabla \cdot \vec{V} = 0 \tag{4e}$$

$$\rho_m(\vec{V} \cdot \nabla)\vec{V} = -\nabla p + \vec{J} \times \vec{B} + \eta \nabla^2 \vec{V} + \rho_e \vec{E} \tag{4f}$$

$$\vec{J} = \sigma_f(\vec{E} + \vec{V} \times \vec{B}) + \rho_e \vec{V} \tag{4g}$$

where $\vec{E}$, $\vec{B}$, $\vec{J}$, ρ_e, ϵ_o, and μ_o are the electric field intensity, magnetic flux density, electric current density, electric charge density, electric permittivity of free-space, and magnetic permeability of free-space, respectively; and $\vec{V}$, ρ_m, η, σ_f, and p are the fluid velocity, density, viscosity, electrical conductivity, and pressure, respectively. (All symbols are also defined in appendix A.) It has been assumed that the permittivity and permeability of the fluid are the same as that of free-space and that the fluid properties ρ_m, η, and σ_f are constant.

It can be shown by using typical values for liquid metal properties that the terms involving the electric charge density ρ_e in equations (4f) and (4g) are negligible compared

with other terms in these equations (ref. 14). The term involving ρ_e in equation (4d) must be retained, however.

Some general properties of the solution of the basic equations can be found without actually solving the equations. Since the pipe cross section and applied magnetic field do not vary along the z-axis, all quantities in the basic equations are independent of z except for the pressure. The pressure consists of the sum of two terms, one linear in z and the second involving an unknown function of x and y (ref. 20). Hence, the axial component of the pressure gradient is a constant. It can also be shown that the fluid velocity has only a z-component V_z and the current density $\vec{J}$ has only x- and y-components. Furthermore, the total magnetic field has only two components - the applied field B_o in the x-direction and an induced field B_z in the z-direction.

Using these general properties of the solution, the basic equations can be reduced to a more manageable set. One approach is to combine all the basic equations yielding one fourth-order equation in V_z. A second, and more preferable, approach which results in two coupled second-order elliptic equations is to eliminate all dependent variables other than V_z and either the induced potential or the induced magnetic field.

First, consider retaining V_z and the induced potential. The induced potential U can be defined as

$$\vec{E} = -\nabla U \tag{5a}$$

Thus, equation (4a) is satisfied for any U. Next, taking the divergence of equation (4b) reveals that

$$\nabla \cdot \vec{J} = 0 \tag{5b}$$

Using this result along with equation (4g) with the $\rho_e \vec{V}$ term omitted as discussed previously then gives

$$\nabla^2 U = \nabla \cdot (\vec{V} \times \vec{B}) \tag{5c}$$

The right side of equation (5c) can be simplified by remembering that $\vec{V}$ has only a z-component and that $\vec{B}$ has only x- and z-components. Thus,

$$\frac{\partial^2 U}{\partial x^2} + \frac{\partial^2 U}{\partial y^2} = B_o \frac{\partial V_z}{\partial y} \tag{5d}$$

is the first of the coupled second-order equations involving only V_z and U. The second equation can be obtained by combining equations (4f), (4g), and (5a) to eliminate $\vec{E}$ and $\vec{J}$

and then taking the z-component of the remaining vector equation giving

$$\frac{\partial^2 V_z}{\partial x^2} + \frac{\partial^2 V_z}{\partial y^2} = \frac{1}{\eta}\frac{\partial p}{\partial z} - \frac{\sigma_f B_o}{\eta}\frac{\partial U}{\partial y} + \frac{\sigma_f B_o^2}{\eta} V_z \tag{5e}$$

An equivalent set of coupled second-order equations involving only V_z and B_z can be obtained in an analogous manner. Taking the curl of equations (4b) and (4g) and combining gives

$$\nabla \times \nabla \times \vec{B} = \mu_o \sigma_f \left[\nabla \times \vec{E} + \nabla \times (\vec{V} \times \vec{B})\right] \tag{5f}$$

Expanding both sides of equation (5f) using standard vector identities and using equations (4a), (4c), and (4e) and known properties of the solution to simplify the result give

$$\frac{\partial^2 B_z}{\partial x^2} + \frac{\partial^2 B_z}{\partial y^2} = -\mu_o \sigma_f B_o \frac{\partial V_z}{\partial x} \tag{5g}$$

The second equation can be obtained by combining equations (4b) and (4f) to eliminate $\vec{J}$ and then taking the z-component of the resulting vector equation giving

$$\frac{\partial^2 V_z}{\partial x^2} + \frac{\partial^2 V_z}{\partial y^2} = \frac{1}{\eta}\frac{\partial p}{\partial z} - \frac{B_o}{\eta \mu_o}\frac{\partial B_z}{\partial x} \tag{5h}$$

The equations just derived apply, of course, only in the fluid. Equations which describe the electromagnetic field in the pipe wall region can be obtained from the previous sets by setting the fluid velocity equal to zero. Thus, for the first set which involves only V_z and U the corresponding equation for the wall region is

$$\frac{\partial^2 U}{\partial x^2} + \frac{\partial^2 U}{\partial y^2} = 0 \tag{5i}$$

Likewise, for the second set which involves only V_z and B_z the corresponding equation

for the wall region is

$$\frac{\partial^2 B_z}{\partial x^2} + \frac{\partial^2 B_z}{\partial y^2} = 0 \tag{5j}$$

In addition to these basic equations, appropriate boundary conditions must be specified to determine the solution uniquely. These conditions are

$$V_z\Big|_{r=a^-} = 0 \tag{6a}$$

$$U\Big|_{r=a^-} = U\Big|_{r=a^+} \tag{6b}$$

$$\frac{1}{\sigma_f} \nabla B_z \cdot \hat{a}_r\Big|_{r=a^-} = \frac{1}{\sigma_w} \nabla B_z \cdot \hat{a}_r\Big|_{r=a^+} \tag{6c}$$

$$\sigma_f \nabla U \cdot \hat{a}_r\Big|_{r=a^-} = \sigma_w \nabla U \cdot \hat{a}_r\Big|_{r=a^+} \tag{6d}$$

$$B_z\Big|_{r=a^-} = B_z\Big|_{r=a^+} \tag{6e}$$

$$\nabla U \cdot \hat{a}_r\Big|_{r=b^-} = 0 \tag{6f}$$

$$B_z\Big|_{r=b^-} = 0 \tag{6g}$$

where $\hat{a}_r$ is the unit vector in the radial direction, σ_w is the electrical conductivity of the wall, and $\Big|_{r=a^-}$ refers to evaluating the quantity preceding it at a radial point just slightly less than $r = a$.

The boundary conditions require the following:

(1) The fluid velocity must be zero along the pipe inner radius (eq. (6a)).

(2) The θ or circumferential component of the electric field must be continuous across the fluid - pipe wall interface at $r = a$ (eqs. (6b) and (6c)).

(3) The radial component of the electric current must be continuous across the fluid - pipe wall interface at $r = a$ (eqs. (6d) and (6e)).

(4) The radial component of the electric current must vanish at the outer pipe radius $r = b$ (eqs. (6f) and (6g)).

Note that although there are only four stated boundary conditions they result in seven equations since equivalent forms involving both U and B_z are given.

When solving the basic equations and associated boundary condition equations, it is convenient to reexpress the equations in the cylindrical coordinate system and to use dimensionless coordinates and dimensionless variables. This can be achieved by introducing the following quantities:

Dimensionless potential:

$$W = \frac{U}{B_o a V_o} \tag{7a}$$

Dimensionless velocity:

$$V = \frac{V_z}{V_o} \tag{7b}$$

Hartmann number:

$$M = B_o a \sqrt{\frac{\sigma_f}{\eta}} \tag{7c}$$

Magnetic Reynolds number:

$$R_m = \mu_o \sigma_f a V_o \tag{7d}$$

Dimensionless axial pressure gradient:

$$P_o = \frac{-a^2}{\eta V_o} \frac{\partial p}{\partial z} \tag{7e}$$

Dimensionless induced magnetic field:

$$B = \frac{B_z}{B_o} \tag{7f}$$

Ratio of wall to fluid conductivity:

$$\gamma = \frac{\sigma_w}{\sigma_f} \tag{7g}$$

Dimensionless radius:

$$\rho = \frac{r}{a} \tag{7h}$$

Ratio of pipe outer-to-inner radii:

$$R = \frac{b}{a} \tag{7i}$$

Characteristic velocity for the flow:

$$V_o \tag{7j}$$

Substituting equations (7a) to (7i) back into the basic equations and boundary conditions then yields the desired equations in dimensionless form. The equations are grouped so that the first set involves only the velocity and induced potential and the second set involves only the velocity and induced magnetic field:

$$\frac{\partial^2 W}{\partial \rho^2} + \frac{1}{\rho}\frac{\partial W}{\partial \rho} + \frac{1}{\rho^2}\frac{\partial^2 W}{\partial \theta^2} = \sin\theta\frac{\partial V}{\partial \rho} + \frac{\cos\theta}{\rho}\frac{\partial V}{\partial \theta} \qquad \rho < 1 \tag{8a}$$

$$\frac{\partial^2 V}{\partial \rho^2} + \frac{1}{\rho}\frac{\partial V}{\partial \rho} + \frac{1}{\rho^2}\frac{\partial^2 V}{\partial \theta^2} = -P_o - M^2\left(\sin\theta\frac{\partial W}{\partial \rho} + \frac{\cos\theta}{\rho}\frac{\partial W}{\partial \theta} - V\right) \qquad \rho < 1 \tag{8b}$$

$$\frac{\partial^2 W}{\partial \rho^2} + \frac{1}{\rho}\frac{\partial W}{\partial \rho} + \frac{1}{\rho^2}\frac{\partial^2 W}{\partial \theta^2} = 0 \qquad 1 < \rho < R \tag{8c}$$

$$V\Big|_{\rho=1^-} = 0 \tag{8d}$$

$$W\Big|_{\rho=1^-} = W\Big|_{\rho=1^+} \tag{8e}$$

$$\frac{\partial W}{\partial \rho}\bigg|_{\rho=1^-} = \gamma \frac{\partial W}{\partial \rho}\bigg|_{\rho=1^+} \tag{8f}$$

$$\frac{\partial W}{\partial \rho}\bigg|_{\rho=R^-} = 0 \tag{8g}$$

$$\frac{\partial^2 B}{\partial \rho^2} + \frac{1}{\rho}\frac{\partial B}{\partial \rho} + \frac{1}{\rho^2}\frac{\partial^2 B}{\partial \theta^2} = -R_m\left(\cos\theta \frac{\partial V}{\partial \rho} - \frac{\sin\theta}{\rho}\frac{\partial V}{\partial \theta}\right) \qquad \rho < 1 \tag{9a}$$

$$\frac{\partial^2 V}{\partial \rho^2} + \frac{1}{\rho}\frac{\partial V}{\partial \rho} + \frac{1}{\rho^2}\frac{\partial^2 V}{\partial \theta^2} = -P_o - \frac{M^2}{R_m}\left(\cos\theta \frac{\partial B}{\partial \rho} - \frac{\sin\theta}{\rho}\frac{\partial B}{\partial \theta}\right) \qquad \rho < 1 \tag{9b}$$

$$\frac{\partial^2 B}{\partial \rho^2} + \frac{1}{\rho}\frac{\partial B}{\partial \rho} + \frac{1}{\rho^2}\frac{\partial^2 B}{\partial \theta^2} = 0 \qquad 1 < \rho < R \tag{9c}$$

$$V\Big|_{\rho=1^-} = 0 \tag{9d}$$

$$\gamma \frac{\partial B}{\partial \rho}\bigg|_{\rho=1^-} = \frac{\partial B}{\partial \rho}\bigg|_{\rho=1^+} \tag{9e}$$

$$B\Big|_{\rho=1^-} = B\Big|_{\rho=1^+} \tag{9f}$$

$$B\Big|_{\rho=R^-} = 0 \tag{9g}$$

Either the set of equations (8a) to (8g) or the set (9a) to (9g) completely specifies the problem.

INDUCED POTENTIAL FOR AN ARBITRARY VELOCITY PROFILE

In this section, a formulation is developed for computing the induced potential for a given but arbitrary velocity profile. The solution is obtained by using the dimensionless equations involving the velocity and induced potential (8a) to (8g). Equation (8b), which relates the fluid velocity to the forces on the fluid, need not be solved, however, since the velocity is assumed to be given. It is also assumed that the given velocity profile vanishes at the pipe wall so that equation (8d) is satisfied.

Induced Potential

The solution for the induced potential can be obtained in a straightforward manner by using a Green's function. The Green's function $G(\rho, \theta \,|\, \rho_o, \theta_o)$ can be defined as the solution of the following equations:

$$\frac{\partial^2 G}{\partial \rho^2} + \frac{1}{\rho}\frac{\partial G}{\partial \rho} + \frac{1}{\rho^2}\frac{\partial^2 G}{\partial \theta^2} = -\frac{1}{\rho_o}\delta(\rho - \rho_o)\delta(\theta - \theta_o) \qquad 0 < \rho < R \tag{10a}$$

$$G\Big|_{\rho=1^-} = G\Big|_{\rho=1^+} \tag{10b}$$

$$\frac{\partial G}{\partial \rho}\bigg|_{\rho=1^-} = \gamma \frac{\partial G}{\partial \rho}\bigg|_{\rho=1^+} \tag{10c}$$

$$\frac{\partial G}{\partial \rho}\bigg|_{\rho=R^-} = 0 \tag{10d}$$

where $\delta(\ )$ is the Dirac delta function.

By properly combining equations (8a) to (8g) with equations (10a) to (10d) and using

Green's second identity it can easily be shown that the dimensionless potential W in the wall region is given by

$$W(\rho,\theta) = \frac{1}{\gamma}\int_0^1\int_0^{2\pi}\left[\sin\theta_o \frac{\partial G}{\partial \rho_o}(\rho_o,\theta_o|\rho,\theta) + \frac{\cos\theta_o}{\rho_o}\frac{\partial G}{\partial \theta_o}(\rho_o,\theta_o|\rho,\theta)\right]$$

$$V(\rho_o,\theta_o)\rho_o\, d\rho_o\, d\theta_o \qquad 1 \le \rho \le R \tag{11}$$

The potential in the fluid region $0 \le \rho \le 1$ is also given by equation (11) with the $1/\gamma$ factor omitted.

The solution for the Green's function is most easily obtained by using Fourier expansion techniques. Since equations (10a) to (10d) reveal that G is an even function of $\theta - \theta_o$, let

$$G(\rho,\theta|\rho_o,\theta_o) = \sum_{n=0}^{\infty} G_n(\rho,\rho_o)\cos n(\theta - \theta_o) \tag{12a}$$

Substituting equation (12a) into (10a) and using the orthogonal properties of the functions $\cos n(\theta - \theta_o)$ $n = 0, 1, 2, \ldots$ over the interval of $\theta - \theta_o$ from 0 to 2π show that $G_n(\rho,\rho_o)$ satisfies the equation

$$\frac{\partial^2 G_n}{\partial \rho^2} + \frac{1}{\rho}\frac{\partial G_n}{\partial \rho} - \frac{n^2}{\rho^2}G_n = -\frac{1}{\pi\rho_o\epsilon_n}\delta(\rho - \rho_o) \tag{12b}$$

where

$$\epsilon_n = \begin{cases} 2 & \text{if } n = 0 \\ 1 & \text{if } n \neq 0 \end{cases}$$

Since the solution of interest is the induced potential in the wall region $1 \le \rho \le R$ due to the fluid motion within the pipe $0 \le \rho \le 1$ it is only necessary to solve equation (12b) for $0 \le \rho \le 1$ and $1 \le \rho_o \le R$. The solution of equation (12b) subject to the boundary conditions (10b) to (10d) is given by

$$G_o(\rho,\rho_o) = 0 \tag{12c}$$

and

$$G_n(\rho,\rho_o) = \frac{\gamma\rho^n\left(\rho_o^n + R^{2n}\rho_o^{-n}\right)}{n\pi\left[(R^{2n}+1) + \gamma(R^{2n}-1)\right]} \qquad n \neq 0 \qquad \begin{matrix} 0 \le \rho \le 1 \\ 1 \le \rho_o \le R \end{matrix} \tag{12d}$$

Thus, substituting equations (12c) and (12d) back into equation (12a) completes the solution for the Green's function. Combining the Green's function solution with equation (11) then yields a formula for computing the potential at any point in the pipe wall due to any fluid velocity profile.

In practice, only the potential difference between points A and D is normally measured (see fig. 2). This potential difference W_{AD} is given by

$$W_{AD} = W(R,\ \pi/2) - W(R,\ -\pi/2) \tag{13a}$$

Combining equations (11) and (13a) and using the Green's function solution just obtained give

$$W_{AD} = \int_0^1\int_0^{2\pi}\sum_{n=1}^{\infty}\frac{4R^n\rho_o^{n-1}\cos(n-1)\theta_o}{\pi\left[(R^{2n}+1)+\gamma(R^{2n}-1)\right]}\sin\frac{n\pi}{2}\,V(\rho_o,\theta_o)\,\rho_o\,d\rho_o\,d\theta_o \tag{13b}$$

Flowmeter Sensitivity

Rather than consider the absolute induced potential difference for a given flow condition, it is more convenient to define a sensitivity for the flowmeter in terms of the potential difference per unit of flow. It is also customary to include the applied magnetic field strength and the pipe inner diameter in the expression for the flowmeter sensitivity. Thus, the flowmeter sensitivity S can be defined as

$$S = \frac{U_{AD}^{(1)}}{2a\,B_o\,V_{zm}} \tag{14a}$$

[1] If the pipe wall is an insulator, the same definition is used for S with U_{AD} and W_{AD} replaced with U_{BC} and W_{BC}, respectively.

where V_{zm}, the mean or average flow velocity, is

$$V_{zm} = \frac{1}{\pi a^2} \int_0^a \int_0^{2\pi} V_z(r, \theta) r \, dr \, d\theta \tag{14b}$$

In terms of the dimensionless variables, S is given by

$$S = \frac{W_{AD}^{(1)}}{2V_m} \tag{14c}$$

where

$$V_m = \frac{1}{\pi} \int_0^1 \int_0^{2\pi} V(\rho, \theta) \rho \, d\rho \, d\theta \tag{14d}$$

Thus, the flowmeter sensitivity for any velocity profile is obtained by combing equations (13b), (14c), and (14d) giving

$$S = \frac{\int_0^1 \int_0^{2\pi} K(\rho, \theta) V(\rho, \theta) \rho \, d\rho \, d\theta}{\int_0^1 \int_0^{2\pi} V(\rho, \theta) \rho \, d\rho \, d\theta} \tag{15a}$$

where

$$K(\rho, \theta) = \sum_{n=1}^{\infty} \frac{2R^n}{(R^{2n} + 1) + \gamma(R^{2n} - 1)} \rho^{n-1} \cos (n - 1)\theta \sin \frac{n\pi}{2} \tag{15b}$$

Equation (15a) is the desired result of this section. It shows that the flowmeter sensitivity is the ratio of the weighted average of the velocity over the pipe cross section to the average velocity with a weighting factor of $K(\rho, \theta)$.

Many of the early results on flowmeter sensitivity can be obtained quite simply from equations (15a) and (15b). First consider the case where the pipe wall is nonconductive.

This corresponds to setting $\gamma = \sigma_w/\sigma_f = 0$ and $R = b/a = 1$. The last step of setting R equal to 1 is a mathematically convenient way of moving the electrodes from points A and D to B and C without redoing the analysis (see fig. 2). It does not require the wall to be infinitely thin. If $R = 1$, γ can actually assume any value since the term involving γ in the expression for $K(\rho, \theta)$ vanishes. Using these values in equation (15b) gives

$$K(\rho, \theta) = \sum_{n=1}^{\infty} \rho^{n-1} \cos (n - 1)\theta \sin \frac{n\pi}{2} \qquad \text{(nonconductive pipe wall)} \tag{16}$$

This immediately shows that if the velocity profile has axial symmetry (i.e., is independent of θ) then only the $n = 1$ term in K, which has unit magnitude, will contribute to the numerator in equation (15a). Thus, a flowmeter with a nonconductive pipe wall and an arbitrary but axially symmetric velocity profile has a sensitivity of 1 or 1 volt of signal, per meter per second of average flow, per weber per square meter of applied magnetic field intensity, per meter of pipe inner diameter. This result has been known for several decades.

Next, consider the case where the velocity profile is still axially symmetric but where the pipe wall is conductive. Again, only the $n = 1$ term in the weighting factor $K(\rho, \theta)$ contributes to the numerator in equation (15a). This time, however, the $n = 1$ term has less than unit magnitude giving a reduced sensitivity of

$$S = \frac{2R}{(R^2 + 1) + \gamma(R^2 - 1)} \tag{17}$$

This sensitivity is less than that for a nonconductive wall since some of the induced output potential is shunted by the conductive wall. This effect was first computed by Elrod and Fouse (ref. 4).

The flowmeter sensitivity for a nonaxially symmetric profile cannot be computed until the profile is specified. However, much can be learned by examining the behavior of the weighting factor $K(\rho, \theta)$ over the pipe cross section. If $K(\rho, \theta)$ were a constant, the flowmeter would be "ideal;" that is, its sensitivity would be completely independent of the velocity profile.

Figures 3 and 4 show typical numerical values for the weighting factor $K(\rho, \theta)$ which result from summing the series in equation (15b).[2] The values shown are normalized

---

[2]The series expression for $K(\rho, \theta)$ given by eq. (15b) can be expressed in closed form only for the case of a nonconductive pipe wall giving

$$K(\rho, \theta) = \frac{1 + \rho^2 \cos 2\theta}{1 + 2\rho^2 \cos 2\theta + \rho^4} \qquad \text{(nonconductive pipe wall)}$$

This result was also obtained by Shercliff (refs. 5 and 6).

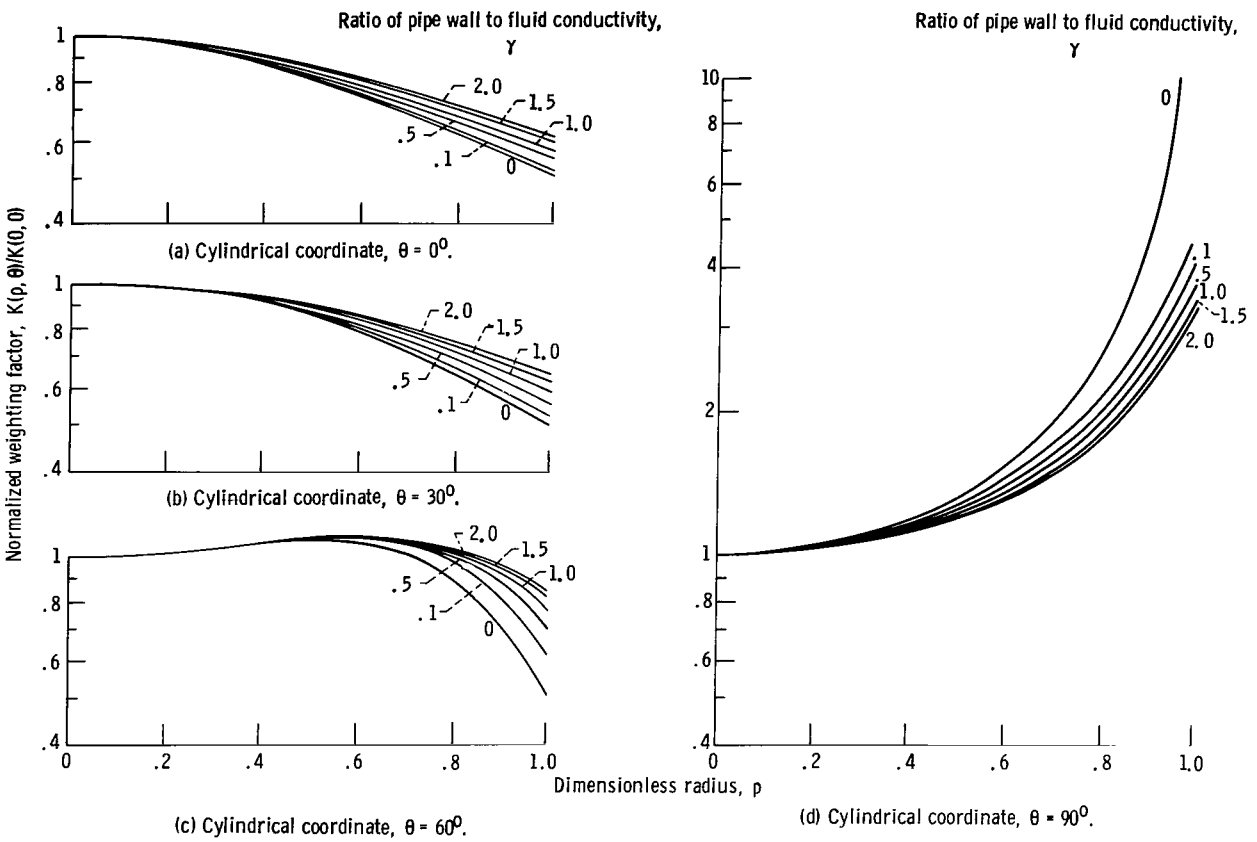

Figure 3. - Flowmeter weighting factor. Ratio of pipe outer-to-inner radii, R = 1.15.

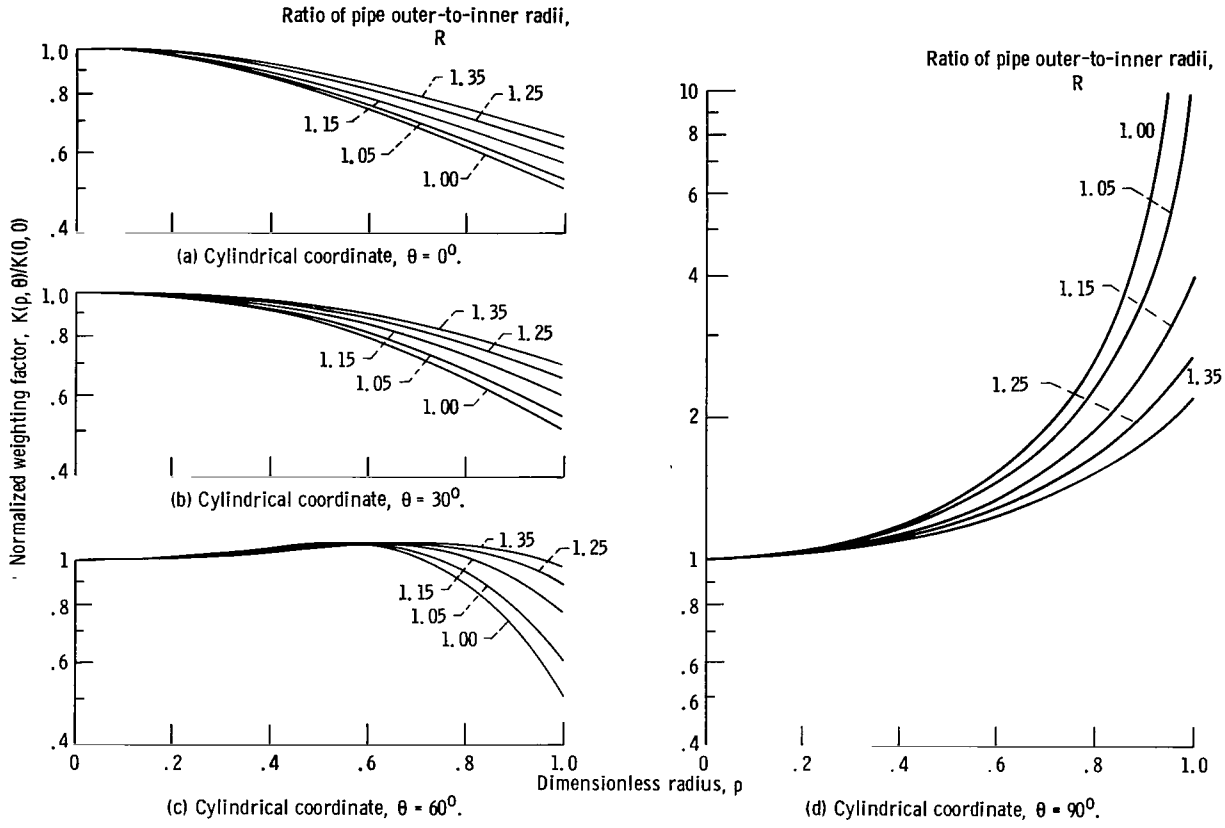

Figure 4. - Flowmeter weighting factor. Ratio of pipe wall to fluid conductivity, $\gamma = 1.00$.

with respect to the weighting factor at the center of the pipe to make the results more easily comparable. The value of the weighting factor at the center $K(0,0)$ is $2R/\left[(R^2+1)+\gamma(R^2-1)\right]$, the pipe shunting factor for axially symmetric flow. Because of symmetry considerations only one quadrant ($0^o \leq \theta \leq 90^o$) need be considered. Figures 3(a) to (d) show the normalized weighting factor as a function of radius at constant θ values of 0^o, 30^o, 60^o, and 90^o, respectively. The pipe outer-to-inner radii ratio R is 1.15 and the wall to fluid conductivity ratio γ is varied from 0 to 2. As shown, the normalized weighting factor is almost constant near the center of the pipe and drops off slowly near the wall for θ less than about 60^o. For $\theta = 90^o$, however, the weighting factor increases quite rapidly with radius and, in fact, becomes infinite at the wall for $\gamma = 0$. The flowmeter output is, therefore, most sensitive to the flow at points near the wall at $\theta \approx 90^o$ and least sensitive to the flow near the wall at $\theta \approx 0^o$. The large ratios of wall to fluid conductivity make the weighting factor closer to that of an ideal flowmeter which has a constant weighting factor.

Figures 4(a) to (d) show additional numerical results for $K(\rho,\theta)$ only this time the ratio of wall to fluid conductivity γ is held constant at 1 and the pipe outer-to-inner radii ratio R is varied. The results show that as the wall thickness increases the weighting factor becomes more nearly a constant.

It can be concluded, therefore, that flowmeters with the highest ratio of pipe outer-to-inner radii and wall to fluid conductivity are the least sensitive to the shape of the fluid velocity profile. This insensitivity to the velocity profile is achieved only at the price of reducing the overall sensitivity since a thick, highly conductive pipe wall gives the largest shunting effect. Thus, the experimenter who can select the pipe wall thickness and conductivity must consider at least two effects in minimizing the flow measurement error. The pipe wall must be sufficiently thick and conductive to minimize errors due to the uncertainty in the exact velocity profile, and at the same time the wall must permit a sufficiently large output potential to minimize the measurement error due to the ambient electrical noise.

As mentioned in the INTRODUCTION, the principal use for the preceding analysis is in the case of low Hartmann number where the velocity profile in the flowmeter is determined by upstream conditions. In the following section, the case where the velocity profile is determined by the flowmeter itself is considered.

INDUCED POTENTIAL FOR FULLY DEVELOPED VELOCITY PROFILE

In this section, the entire set of basic equations will be solved simultaneously to obtain the self-consistent solution for the fully developed velocity profile and the corre-

sponding induced potential. From these results the flowmeter sensitivity can be easily computed.

Two approaches will be followed. First, an exact series representation of the solution will be obtained, and second, an approximate solution using a variational principle and the Ritz technique will be computed. The exact series solution can be summed numerically using modern computers only for Hartmann numbers M less than 10 to 20, whereas the solution found using the variational principle can be evaluated at all Hartmann numbers. The exact series solution is of value, however, since it gives some insight on the accuracy of approximate solution in the lower Hartmann number range. In addition, it is much faster computationally to use the series solution where it applies. Finally, by using transformation techniques such as the Watson transform it may be possible to transform the exact series solution which converges slowly at high Hartmann numbers into one which converges rapidly.

Exact Series Solution

Solution of basic equations. - In obtaining the series representation of the solution it is convenient to work with equations (9a) to (9g) which involve only the velocity and induced magnetic field. Equations (9a) and (9b) can be uncoupled by introducing the auxiliary functions f and g where

$$V(\rho,\theta) = \frac{1}{2}\left[e^{-\frac{M}{2}\rho\cos\theta} f(\rho,\theta) + e^{\frac{M}{2}\rho\cos\theta} g(\rho,\theta)\right] \tag{18a}$$

$$B(\rho,\theta) = \frac{R_m}{2M}\left[e^{-\frac{M}{2}\rho\cos\theta} f(\rho,\theta) - e^{\frac{M}{2}\rho\cos\theta} g(\rho,\theta)\right] - \frac{P_o R_m}{M^2}\rho\cos\theta \tag{18b}$$

Substituting equations (18a) and (18b) back into equations (9a) and (9b) reveals that f and g must satisfy the following equations:

$$\frac{\partial^2 f}{\partial\rho^2} + \frac{1}{\rho}\frac{\partial f}{\partial\rho} + \frac{1}{\rho^2}\frac{\partial^2 f}{\partial\theta^2} - \frac{M^2}{4} f = 0 \tag{19a}$$

$$\frac{\partial^2 g}{\partial \rho^2} + \frac{1}{\rho}\frac{\partial g}{\partial \rho} + \frac{1}{\rho^2}\frac{\partial^2 g}{\partial \theta^2} - \frac{M^2}{4} g = 0 \tag{19b}$$

The general solution for f and g can be expressed as a Fourier series in θ. Symmetry considerations show that both V and B, and, hence, f and g, must be even functions of θ about $\theta = 0$. Thus, only cos $n\theta$ type terms need appear in the series. The coefficients in the Fourier series are, in general, linear combinations of the modified Bessel functions with argument $M\rho/2$. Since modified Bessel functions of the second kind diverge at zero argument, they must be excluded. Thus, the solutions to equations (19a) and (19b) are given by

$$f(\rho, \theta) = \sum_{n=0}^{\infty} A_n I_n\left(\frac{M}{2}\rho\right) \cos n\theta \tag{20a}$$

$$g(\rho, \theta) = \sum_{n=0}^{\infty} B_n I_n\left(\frac{M}{2}\rho\right) \cos n\theta \tag{20b}$$

where A_n and B_n are constants to be determined. Combining the solutions for f and g with equations (18a) and (18b) give the general solution for V and B in the fluid region $0 \le \rho \le 1$:

$$V(\rho, \theta) = \frac{1}{2} \sum_{n=0}^{\infty} \left(e^{-\frac{M}{2}\rho \cos\theta} A_n + e^{\frac{M}{2}\rho \cos\theta} B_n \right) I_n\left(\frac{M}{2}\rho\right) \cos n\theta \qquad 0 \le \rho \le 1 \tag{21a}$$

$$B(\rho, \theta) = \frac{1}{2}\frac{R_m}{M} \sum_{n=0}^{\infty} \left(e^{-\frac{M}{2}\rho \cos\theta} A_n - e^{\frac{M}{2}\rho \cos\theta} B_n \right) I_n\left(\frac{M}{2}\rho\right) \cos n\theta$$

$$- \frac{P_o R_m}{M^2} \rho \cos\theta \qquad 0 \le \rho \le 1 \tag{21b}$$

In the pipe wall region $1 \leq \rho \leq R$ the induced magnetic field satisfies equation (9c) which is Laplace's equation. The solution of this equation which satisfies boundary condition (9g) can also be found using Fourier expansion techniques and is given by

$$B(\rho, \theta) = \sum_{n=1}^{\infty} C_n(\rho^n - R^{2n}\rho^{-n}) \cos n\theta \qquad 1 \leq \rho \leq R \tag{21c}$$

where the C_n are constants to be determined.

The unknown constants A_n, B_n, and C_n can be determined by requiring the general solutions given by equations (21a), (21b), and (21c) to satisfy the three remaining boundary conditions (9d), (9e), and (9f). Substituting equations (21a) to (21c) into equations (9d) to (9f) and using the orthogonal properties of the $\cos n\theta (n = 0, 1, 2, \ldots)$ functions over the interval $0 \leq \theta \leq 2\pi$ and the integral definition of the modified Bessel functions

$$I_n\left(\frac{M}{2}\right) = \frac{1}{2\pi} \int_0^{2\pi} e^{\frac{M}{2}\cos\theta} \cos n\theta \, d\theta \tag{22}$$

give the following relations:

$$C_n = 0 \qquad n \text{ even} \tag{23a}$$

$$C_n = -\frac{\gamma}{n(R^{2n}+1)}\left[\frac{R_m P_o}{M^2}\delta_{1n} + \frac{R_m P_o}{2M} T_n\left(\frac{M}{2}\right) + \frac{M}{4}\sum_{k=1,3,5,\ldots}^{\infty} (1 - R^{2k}) S_{nk}\left(\frac{M}{2}\right) C_k\right] \qquad n \text{ odd} \tag{23b}$$

$$A_n = \frac{1}{\pi \epsilon_n I_n\left(\frac{M}{2}\right)} \left\{ \frac{\pi M}{R_m} \sum_{k=1,3,5,\ldots}^{\infty} (1 - R^{2k}) \left[I_{k+n}\left(\frac{M}{2}\right) + I_{k-n}\left(\frac{M}{2}\right) \right] C_k \right.$$

$$\left. + \frac{2P_o \pi}{M} I'_n\left(\frac{M}{2}\right) \right\} \tag{23c}$$

$$B_n = (-1)^n A_n \tag{23d}$$

$$T_n\left(\frac{M}{2}\right) = \sum_{k=0}^{\infty} (-1)^k (2 - \delta_{0k}) I'_k\left(\frac{M}{2}\right) \left\{ \frac{I'_k\left(\frac{M}{2}\right)}{I_k\left(\frac{M}{2}\right)} \left[I_{n+k}\left(\frac{M}{2}\right) + I_{n-k}\left(\frac{M}{2}\right) \right] \right.$$

$$\left. + I'_{n+k}\left(\frac{M}{2}\right) + I'_{n-k}\left(\frac{M}{2}\right) \right\} \tag{23e}$$

$$S_{nk}\left(\frac{M}{2}\right) = \sum_{m=0}^{\infty} (-1)^m (2 - \delta_{0m}) \left[I_{k+m}\left(\frac{M}{2}\right) + I_{k-m}\left(\frac{M}{2}\right) \right]$$

$$\cdot \left\{ \frac{I'_m\left(\frac{M}{2}\right)}{I_m\left(\frac{M}{2}\right)} \left[I_{n+m}\left(\frac{M}{2}\right) + I_{n-m}\left(\frac{M}{2}\right) \right] + I'_{n+m}\left(\frac{M}{2}\right) + I'_{n-m}\left(\frac{M}{2}\right) \right\} \tag{23f}$$

where

$$\delta_{ij} = \begin{cases} 1 & \text{if } i=j \\ 0 & \text{if } i \neq j \end{cases}$$

and the prime (') denotes differentiation with respect to the argument of the modified Bessel functions.

These equations show that the C_n ($n = 1,3,5,\ldots$), which are the coefficients in the expansion for the induced magnetic field in the pipe wall, satisfy an infinite set of linear algebraic equations. The solution for the C_n can be obtained by truncating the infinite set at a sufficiently large n and then solving the remaining finite set using standard techniques. It should be noted that in this set of equations both the inhomogeneous terms, $T_n(M/2)$, and the coefficients of the C_n terms, $S_{nk}(M/2)$, involve infinite series (see eqs. (23e) and (23f)). These infinite series, however, involve only the Hartmann number M and are independent of the conductivity and radius ratios γ and R. Thus, the series need be summed only once for each M of interest.

Once the C_n have been determined, it is then quite straightforward to compute the A_n using equation (23c) and the B_n from equation (23d). The velocity and induced magnetic field can then be found from equations (21a) to (21c). Before presenting numerical results, expressions for the average velocity, induced potential, and flowmeter sensitivity will be obtained. In addition, the limiting case of low M will be considered.

Average velocity and induced potential. - The flowmeter sensitivity, in terms of the dimensionless variables, is the ratio of the potential difference W_{AD} to twice the mean velocity V_m (see eq. (14c)). Thus, to compute the sensitivity for the series solution just obtained it is necessary to relate the induced potential to the velocity and induced magnetic field. This is most easily done by first computing the electric field and then evaluating the line integral of the electric field from one electrode to the other to obtain the potential difference. Since the answer is independent of the path of integration, it is most convenient to use the circumferential path along the outer surface of the pipe wall.

In the pipe wall region, Maxwell's equations and Ohm's law can be combined to give

$$\nabla \times \vec{B} = \mu_o \vec{J} = \mu_o \sigma_w \vec{E} = -\mu_o \sigma_w \nabla U \tag{24a}$$

Since the path of integration corresponds to a constant radius, only $\partial U/\partial\theta$ need be evaluated:

$$\frac{\partial U}{\partial \theta} = -\frac{r}{\mu_o \sigma_w}(\nabla \times \vec{B}) \cdot \hat{a}_\theta = \frac{r}{\mu_o \sigma_w} \frac{\partial B_z}{\partial r} \tag{24b}$$

Reexpressing equation (24b) in terms of the dimensionless variables then yields

$$\frac{\partial W}{\partial \theta} = \frac{\rho}{\gamma R_m} \frac{\partial B}{\partial \rho} \tag{24c}$$

The potential difference W_{AD} can be computed by integrating equation (24c) with respect to θ from $-\pi/2$ to $\pi/2$ along the curve $\rho = R$:

$$W_{AD} = \frac{R}{\gamma R_m} \int_{-\pi/2}^{+\pi/2} \left. \frac{\partial B}{\partial \rho} \right|_{\rho=R^-} d\theta \tag{24d}$$

Combining this expression for W_{AD} with the general solution for B in the wall region (eq. (21c)) then gives

$$W_{AD} = \frac{4}{\gamma R_m} \sum_{n=1,3,5,\ldots}^{\infty} C_n R^n \sin \frac{n\pi}{2} \tag{25}$$

The average dimensionless velocity V_m can be obtained by combining the definition for the average (see eq. (14d)) with the general solution for V given by equation (21a) and performing the integration with respect to ρ and θ. This gives

$$V_m = \sum_{n=0}^{\infty} (-1)^n A_n \left[\frac{(M^2 + 4n^2)}{M^2} I_n^2\left(\frac{M}{2}\right) - I_n'^2\left(\frac{M}{2}\right) \right] \tag{26}$$

where equation (23d) was used to eliminate the B_n terms. The flowmeter sensitivity is then simply the ratio of W_{AD} (eq. (25)) to twice V_m (eq. (26)).

Asymptotic solution for small M. - Results for the limiting case of low Hartmann number can be obtained by expressing $T_n(M/2)$ and $S_{nk}(M/2)$ in a power series in M by using the asymptotic form for the modified Bessel functions for small argument. Substituting these expansions into the set of equations for the C_n (eq. (23b)) then gives

$$C_1 = \frac{\gamma R_m P_o}{8\left[(R^2 + 1) + \gamma(R^2 - 1)\right]} \left\{ 1 - \frac{M^2}{48} - \frac{\gamma(R^2 - 1)M^2}{8\left[(R^2 + 1) + \gamma(R^2 - 1)\right]} + \ldots \right\} \tag{27a}$$

$$C_3 = \frac{\gamma R_m P_o M^2}{4608\left[(R^6 + 1) + \gamma(R^6 - 1)\right]} \left\{ 1 + \ldots \right\} \tag{27b}$$

$$C_n = \frac{\gamma R_m P_o M^{n-1}}{2^{2n}\, n(n+1)!\left[(R^{2n} + 1) + \gamma(R^{2n} - 1)\right]} \left\{ 1 + \ldots \right\} \qquad n \geq 5 \tag{27c}$$

Knowing the C_n, it is then quite simple to compute the A_n using equation (23c):

$$A_o = P_o \left\{ \frac{1}{4} - \frac{M^2}{128} - \frac{\gamma(R^2 - 1)M^2}{32\left[(R^2 + 1) + \gamma(R^2 - 1)\right]} + \ldots \right\} \tag{27d}$$

$$A_1 = P_o \left\{ \frac{4}{M^2} + \frac{1}{4} - \frac{\gamma(R^2 - 1)}{2\left[(R^2 + 1) + \gamma(R^2 - 1)\right]} + \ldots \right\} \tag{27e}$$

$$A_2 = P_o \left\{ \frac{8}{M^2} + \ldots \right\} \tag{27f}$$

$$A_n = P_o \left\{ \frac{4n}{M^2} + \ldots \right\} \qquad n \geq 3 \tag{27g}$$

Substituting these results for the C_n and A_n into the general expressions for the induced potential difference W_{AD}, the average velocity V_m, and the sensitivity S then gives

$$W_{AD} = \frac{P_o R}{2\left[(R^2 + 1) + \gamma(R^2 - 1)\right]} \left\{ 1 - \frac{M^2}{48} - \frac{\gamma(R^2 - 1)M^2}{8\left[(R^2 + 1) + \gamma(R^2 - 1)\right]} \right.$$

$$\left. - \frac{R^2 M^2}{576} \frac{\left[(R^2 + 1) + \gamma(R^2 - 1)\right]}{\left[(R^6 + 1) + \gamma(R^6 - 1)\right]} + \ldots \right\} \tag{28a}$$

$$V_m = \frac{P_o}{8} \left\{ 1 - \frac{M^2}{48} - \frac{\gamma(R^2 - 1)M^2}{8\left[(R^2 + 1) + \gamma(R^2 - 1)\right]} + \ldots \right\} \tag{28b}$$

$$S = \frac{2R}{\left[(R^2 + 1) + \gamma(R^2 - 1)\right]} \left\{ 1 - \frac{M^2 R^2}{576} \left[\frac{(R^2 + 1) + \gamma(R^2 - 1)}{(R^6 + 1) + \gamma(R^6 - 1)} \right] + \ldots \right\} \tag{28c}$$

This same result has also been obtained by Shercliff (ref. 11) who used an iterative procedure. The first term in the expression for the sensitivity is recognized as the pipe wall shunting factor. The results show that the fully developed velocity profile at low M causes a decrease in the sensitivity. Equation (28c) gives useful numerical results (within 1 percent) for $M \leq 4$. Extending the results in the same manner including terms that vary as M^4 expands the useful range to only $M \leq 4.5$. In the next section, a numerical evaluation of the exact series solution is presented.

Numerical results for exact series solution. - The infinite series for $T_n(M/2)$ and $S_{nk}(M/2)$ were summed using an IBM 7094 computer and double precision arithmetic. The modified Bessel functions were evaluated to at least 14 place accuracy. The principle difficulty in summing these series for $T_n(M/2)$ and $S_{nk}(M/2)$ is that the terms alternate in sign and the values of the sums are normally many orders of magnitude less than the magnitude of the largest term in the series. To obtain a minimum of 3 to 4 place accuracy for $T_n(M/2)$ and $S_{nk}(M/2)$ the values for n, k, and M were restricted to where the values for $T_n(M/2)$ and $S_{nk}(M/2)$ were at least 10^{-9} to 10^{-10} times the largest term in their respective series. This restricted n and k to be less than 19 for M of 5 and 10, and less than 11 for M of 20.

The limitation on the maximum values permitted for n and k for a given M immediately determines the maximum number at which the infinite set of equations for the C_n

must be truncated. A detailed study of these equations reveals that they are diagonally dominant, at least for $M \leq 20$. The computed value of C_1, for example, was found to be almost independent of the number of equations used. Thus, the values obtained for the C_n are accurate, but the number of C_n that can be computed is limited.

The next difficulty arose in evaluating the A_n given by equation (23c) because of the infinite series. Often this series did not converge using the finite number of C_n available. The nonconductive pipe wall case ($R = 1$) presented no trouble at this point since the series vanishes so that A_n could be computed for any n. However, as the pipe wall thickness and conductivity and the Hartmann number are increased, the maximum number of A_n that can be computed decreases since there are insufficient numbers of C_n available to sum the series. For example, using the thickest wall ($R = 1.35$) and largest conductivity ratio of interest ($\gamma = 2.0$) permits the A_n up to A_{16} to be calculated to 4 place accuracy at $M = 10$ but only up to A_6 to the same accuracy at $M = 20$.

Additional limitations occurred in evaluating the velocity profile, the induced potential difference W_{AD}, the average velocity V_m, and the ratio $W_{AD}/2V_m$ which is the flowmeter sensitivity. There were insufficient numbers of A_n available to evaluate the series solution for the velocity profile (eq. (21a)) at $M = 20$ except for the case of a nonconductive pipe wall. As the pipe wall thickness and conductivity increased, the values for M had to be restricted in order to sum the series to 4 place accuracy with the finite number of terms available. For thickest and most highly conductive pipe wall case considered ($R = 1.35$, $\gamma = 2.0$), the velocity profile series could only be summed for $M \leq 12$.

The infinite series for the average velocity over the pipe cross section (eq. (26)) converged faster than the series for the velocity at any given point in the cross section. The series for V_m could be evaluated to at least 5 place accuracy for $M \leq 10$ and to a maximum error of a few parts in the third place at $M = 20$. The series for the induced potential difference W_{AD} converged rapidly for $M \leq 20$ and presented no difficulty.

The numerical results are presented in table I for M values of 1, 2, 5, 10, and 20. The values are accurate to the 3 places shown except at $M = 20$ where the third place may be in error. The values used for the ratio of the outer-to-inner pipe radii R are 1.00, 1.05, 1.15, 1.25, and 1.35 and the values used for the wall to fluid conductivity ratio γ are 0, 0.1, 0.5, 1.0, 1.5, and 2.0. The motivation for selecting these particular values is presented in appendix B.

Results are given for V_m/P_o, W_{AD}/P_o, $S(=W_{AD}/2V_m)$, and the "distortion factor" F_D. The distortion factor F_D is related to the flowmeter sensitivity by

$$S = \frac{2R}{(R^2 + 1) + \gamma(R^2 - 1)} F_D(R, \gamma, M) \tag{29}$$

It is introduced to clearly separate the two causes for reduced sensitivity. The first is simply the electrical shunting effect of the induced output potential by the conductive pipe wall for the axially symmetric profile. This is the first term in equation (29), and it is independent of M. The factor F_D accounts for the change in sensitivity due to the distortion of the velocity profile from axial symmetry by the applied static magnetic field.

The results in table I show that the distortion factor F_D, which is 1 at $M = 0$, decreases as M increases. This result is in agreement with the asymptotic solutions for small M given in the previous section. What is surprising, however, is that F_D decreases more rapidly with increasing M if R and γ are small. This is not expected since small values for R and γ produce the least distortion in the velocity profile at low M and, hence, are expected to yield the smallest change in F_D. However, the previous section, which considered the effect of an arbitrary velocity profile, showed that flowmeters with small R and γ are the most sensitive to distortions in the velocity profile from axial symmetry. Thus, even though flowmeters with small R and γ produce the least distortion for $M \leq 20$, they produce the largest change in the distortion factor F_D.

The remaining entries in table I show that both V_m/P_o and W_{AD}/P_o decrease with increasing M and that the decrease is more rapid for large R and γ. This effect is due to the increase in P_o which is proportional to the pressure drop per unit length along the pipe. As M increases, the velocity profile distorts from its Poiseuille profile resulting in a larger viscous drag force. In addition, if the pipe wall is conductive, some of the induced current, which must form a closed path, can return through the pipe wall rather than only through the fluid, thus giving a net electromagnetic drag force on the fluid. The increase in these forces must be balanced by a corresponding increase in P_o to maintain the same flow. The values for V_m/P_o can be used to predict the pressure drop across a flowmeter. However, it must be remembered that the tabulated values are only for the fully developed region. Appropriate amounts must be included for the entry and exit regions to obtain the total pressure drop.

In the next section, an approximate solution is obtained using a variational principle and the Ritz technique.

Approximate Solution Using Variational Principle and Ritz Technique

Variational principle. - An alternative approach for obtaining a solution is to convert the problem of solving the governing differential equations and associated boundary conditions into an equivalent variational problem. It can be shown (refs. 16 and 17) that the Euler-Lagrange equations and natural boundary conditions of the functional F are the basic equations and boundary conditions (8a) to (8g) where F is given by

$$F = \int_0^1 \int_0^{2\pi} \left\{ 2P_o V - \left(\frac{\partial V}{\partial \rho}\right)^2 - \frac{1}{\rho^2}\left(\frac{\partial V}{\partial \theta}\right)^2 - M^2 \left[V^2 + \left(\frac{\partial W}{\partial \rho}\right)^2 + \frac{1}{\rho^2}\left(\frac{\partial W}{\partial \theta}\right)^2 - 2 \sin\theta \, V \frac{\partial W}{\partial \rho} - \frac{2}{\rho} \right.\right.$$

$$\left.\left. \times \cos\theta \, V \frac{\partial W}{\partial \theta} \right] \right\} \rho \, d\rho \, d\theta - \gamma M^2 \int_1^R \int_0^{2\pi} \left[\left(\frac{\partial W}{\partial \rho}\right)^2 + \frac{1}{\rho^2}\left(\frac{\partial W}{\partial \theta}\right)^2 \right] \rho \, d\rho \, d\theta$$

$$+ 2 \int_0^{2\pi} V \frac{\partial V}{\partial \rho}\bigg|_{\rho=1^-} d\theta \tag{30}$$

The functional F has the property that its first variation is zero. Thus, F is stationary; that is, first-order changes in V and W about their true values produce only second-order changes in F. It can also be shown that of all functions that are continuous with piecewise continuous first derivatives, the particular functions for V and W that make F stationary satisfy equations (8a) to (8g) and, hence, are the desired solutions.

A very important property of the functional F (refs. 16 and 17) is that its stationary value F_{st} is given by

$$F_{st} = P_o \int_0^1 \int_0^{2\pi} V \rho \, d\rho \, d\theta \tag{31}$$

Since the dimensionless pressure gradient P_o is a constant, the stationary value for F is proportional to the average fluid velocity in the pipe. This is a very useful result since the average velocity is one of the quantities needed to obtain the flowmeter sensitivity. The stationary value of F can normally be computed to good accuracy by using approximate functions for V and W.

A careful study of equation (30) reveals that the stationary value of F is not an extremum. However, if the class of admissible functions for V is restricted so that either V or $\partial V/\partial \rho$ is specified at $\rho = 1^-$, then it can be shown that the stationary value for F is a maximum (refs. 16 and 17). Thus, if F is maximized over a subset of the entire class of admissible functions for V and W subject to this restriction, the resulting stationary value when used in conjunction with equation (31) will give a computed average velocity which is less than or equal to the actual average velocity. The proper restric-

tion to impose is to require all admissible functions for V to be zero at $\rho = 1^-$ which is boundary condition (8d).

Ritz technique. - Approximate solutions for the velocity and potential will be obtained using the Ritz technique. In this technique, the velocity and potential are expressed in terms of known functions of ρ and θ that approximate the true solution but contain adjustable parameters $\Omega_1, \ldots, \Omega_n$. Substituting this approximate solution into equation (30) and performing the integrations over ρ and θ then leave F as a function of the adjustable parameters $\Omega_1, \ldots, \Omega_n$ and the characteristic parameters of the model P_o, M, γ, and R. Assuming that the approximate solution for V vanishes at $\rho = 1^-$ for all values of $\Omega_1, \ldots, \Omega_n$, the stationary value of F can be found by maximizing F with respect to $\Omega_1, \ldots, \Omega_n$. The corresponding values for $\Omega_1, \ldots, \Omega_n$ at the stationary point, when substituted into the approximate functions for V and W, will yield the closest approximations to the velocity and potential that are possible for the class of functions used.

It is convenient to express the general solutions for V and W by the following Fourier expansions:

$$V(\rho, \theta) = \sum_{n=0}^{N} f_n(\rho) \cos 2n\theta \tag{32a}$$

$$W(\rho, \theta) = \sum_{n=0}^{N} g_n(\rho) \sin (2n + 1)\theta \tag{32b}$$

where the radial functions f_n and g_n are to be determined. Symmetry considerations show that the $\cos 2n\theta$ and $\sin (2n + 1)\theta$ functions with $n = 0, 1, 2, \ldots \infty$ are complete for V and W, respectively. Substituting expansions (32a) and (32b) into equation (30) and performing the integration over θ then give

$$F = \pi \sum_{n=0}^{N} \left(\int_0^1 \left\{ 4P_o \delta_{n0} f_n - \epsilon_n \left(\frac{df_n}{d\rho}\right)^2 - \frac{4n^2}{\rho^2} f_n^2 - M^2 \left[\epsilon_n f_n^2 + \left(\frac{dg_n}{d\rho}\right)^2 + \frac{(2n+1)^2}{\rho^2} g_n^2 \right. \right. \right.$$

$$\left. \left. \left. - (\epsilon_n f_n - f_{n+1}) \frac{dg_n}{d\rho} - \frac{(2n+1)}{\rho} (\epsilon_n f_n + f_{n+1}) g_n \right] \right\} \rho \, d\rho - \gamma M^2 \int_1^R \left[\left(\frac{dg_n}{d\rho}\right)^2 + \frac{(2n+1)^2}{\rho^2} g_n^2 \right] \rho \, d\rho + 2\epsilon_n f_n \left. \frac{df_n}{d\rho} \right|_{\rho=1^-} \right) \tag{33}$$

Each of the radial functions f_n and g_n can be expressed in series form as

$$f_n(\rho) = \sum_{i=1}^{I_n} A_{ni}\rho^{\alpha_{ni}} \qquad n = 0,1,2, \ldots, N;\ 0 \le \rho \le 1 \tag{34a}$$

$$g_n(\rho) = \sum_{j=1}^{J_n} C_{nj}\rho^{\beta_{nj}} \qquad n = 0,1,2, \ldots, N;\ 0 \le \rho \le R \tag{34b}$$

Since the functions $\rho^n (n = 0,1,2, \ldots, \infty)$ form a complete set with respect to functions that are continuous with piecewise continuous derivatives, the exact solution can be obtained by setting $\alpha_{ni} = i - 1$, $\beta_{nj} = j - 1$, $N = \infty$, $I_n = \infty$, and $J_n = \infty$, by substituting equations (34a) and (34b) into equation (33), and by finding the stationary point of F by solving

$$\frac{\partial F}{\partial A_{ni}} = 0 \qquad n = 0,1,2, \ldots, N;\ i = 1,2,3, \ldots, I_n \tag{35a}$$

$$\frac{\partial F}{\partial C_{nj}} = 0 \qquad n = 0,1,2, \ldots, N;\ j = 1,2,3, \ldots, J_n \tag{35b}$$

for A_{ni} and C_{nj}. The solution of this doubly infinite set of equations yields the exact solution to the problem. In practice, these equations are solved by first truncating the sets at some arbitrary upper limit and solving the resulting equations. The upper limit is then increased and the process is repeated until the sequence of solutions converges. Convergence to the correct solution is assured since the functions used in the expansions form complete sets.

The main difficulty with this technique is that, for large M, the number of equations to be solved of the form (35a) and (35b) become prohibitively large before convergence is achieved. The reason for this difficulty at high Hartmann number is that the functions f_n, for example, are normally very small for $\rho < 1 - (1/M)$ (except for f_0) and become large and oscillatory with ρ for $1 - (1/M) < \rho < 1$. It takes a large number of functions of the form ρ^n $(n = 0,1,2, \ldots)$ to represent a function with this behavior.

It was found, however, that if the exponents α_{ni} and β_{nj} in the trial functions (34a) and (34b) are also considered as adjustable parameters rather than fixed integers then convergence is achieved with a manageable number of equations. Thus, in addition to

solving equations (35a) and (35b), equations of the form

$$\frac{\partial F}{\partial \alpha_{ni}} = 0 \qquad n = 0,1,2, \ldots, N;\ i = 1,2,3, \ldots, I_n \tag{35c}$$

$$\frac{\partial F}{\partial \beta_{nj}} = 0 \qquad n = 0,1,2, \ldots, N;\ j = 1,2,3, \ldots, J_n \tag{35d}$$

must also be solved. Since the exponents are variables, completeness of the set of expansion functions is no longer assured. However, this is not a serious drawback since much is known about the general form of the solution and various tests are available for checking the results.

In order to further minimize the number of equations to be solved, several of the known properties of the solution were built into the trial functions. In the pipe wall region, the radial functions g_n which satisfy equations (8c), (8e), and (8g) are given by

$$g_n(\rho) = \frac{\rho^{2n+1} + R^{4n+2}\,\rho^{-(2n+1)}}{1 + R^{4n+2}} \sum_{j=1}^{J_n} C_{nj} \qquad n = 0,1,2, \ldots, N;\ 1 \le \rho \le R \tag{36a}$$

Thus, the expression for g_n given by equation (34b) is used only over the interval $0 \le \rho \le 1$ and equation (36a) is used for g_n for $1 \le \rho \le R$. In addition, the boundary condition which requires V to vanish at $\rho = 1^-$ can be built into the trial functions quite simply by setting $f_n(1) = 0$ or

$$\sum_{i=1}^{I_n} A_{ni} = 0 \qquad n = 0,1,2, \ldots, N \tag{36b}$$

Equation (36b) ensures that the stationary point of F is a maximum. Thus, rather than solving equations (35a) to (35d) to obtain the stationary point, an alternative approach is to maximize F with respect to the A_{ni}, C_{nj}, α_{ni}, and β_{nj} subject to the constraint given by equation (36b).

Evaluation of solution. - In most applications of the Ritz technique, the adjustable parameters are restricted to the linear coefficients such as the A_{ni} and C_{nj} in equations (34a) and (34b). The equations to be solved for the stationary point ((35a) and (35b)) are, therefore, linear in the adjustable parameters since f_n and g_n appear in F only

to the second power. The solution is thus reduced to solving a system of simultaneous linear algebraic equations.

Allowing the exponents in equations (34a) and (34b) to vary still results in linear equations for the A_{ni} and C_{nj} ((35a) and (35b)) but they are nonlinear in α_{ni} and β_{nj}. In addition, the other equations that are introduced ((35c) and (35d)) are nonlinear in all variables.

Rather than attempt to solve these nonlinear equations, it was found simpler to maximize F directly. This was done by using the search technique developed by Powell (ref. 21) which finds the minimum of a function of several variables without calculating derivatives. (Maximizing F is the same as minimizing -F.) This technique was used primarily to determine how many adjustable parameters were needed for convergence as a function of M, R, and γ. The problem was repeatedly solved for increasing values of N, I_n, and J_n where N is the upper limit in the summation over the angular index n (see eqs. (32), (33), and (34)) and I_n and J_n are the upper limits in the summations over the radial indices (see eqs. (34a) and (34b)). The process was terminated when an increase in N, I_n, and J_n did not produce a corresponding increase in the maximum value for F.

It was found that at a given Hartmann number, the largest number of parameters required for convergence occurred when the pipe wall was nonconductive (i.e., R = 1.0, γ = 0). The number of parameters was then fixed at the value required for convergence in the nonconductive pipe wall case when evaluating results for other values of R and γ at the same M. Table II shows the number of parameters used at each value of M.

Although this technique for maximizing F worked well even if the initial guess was poor, it was too slow for computing all the results. Consequently, once the solution for the nonconductive pipe wall case at each M was determined, a modification of another technique developed by Powell (ref. 22) for solving systems of nonlinear algebraic equations was used. This technique, which is a combination of Newton's method and the method of steepest descents, was used to solve equations (35a) to (35d) as follows:

(1) Using the best guess available for the exponents α_{ni} and β_{nj}, equations (35a), (35b), and (36b) were solved exactly for A_{ni} and C_{nj}. This could be done quite rapidly since these equations are linear algebraic equations in A_{ni} and C_{nj}.

(2) The solution for the A_{ni} and C_{nj} with the corresponding values for α_{ni} and β_{nj} were then used to evaluate $\partial F/\partial \alpha_{ni}$ and $\partial F/\partial \beta_{nj}$ (left sides of eqs. (35c) and (35d)).

(3) Powell's technique was then used to compute values for α_{ni} and β_{nj} that satisfied equations (35c) and (35d). Each time new values of $\partial F/\partial \alpha_{ni}$ and $\partial F/\partial \beta_{nj}$ were required steps (1) and (2) were repeated.

(4) The iterative procedure was terminated when the sum of the squares of $\partial F/\partial \alpha_{ni}$ and $\partial F/\partial \beta_{nj}$ was less than a cutoff value which was typically 10^{-16} to 10^{-20}.

(5) After completing steps (1) to (4) for given values of R and γ, the process was

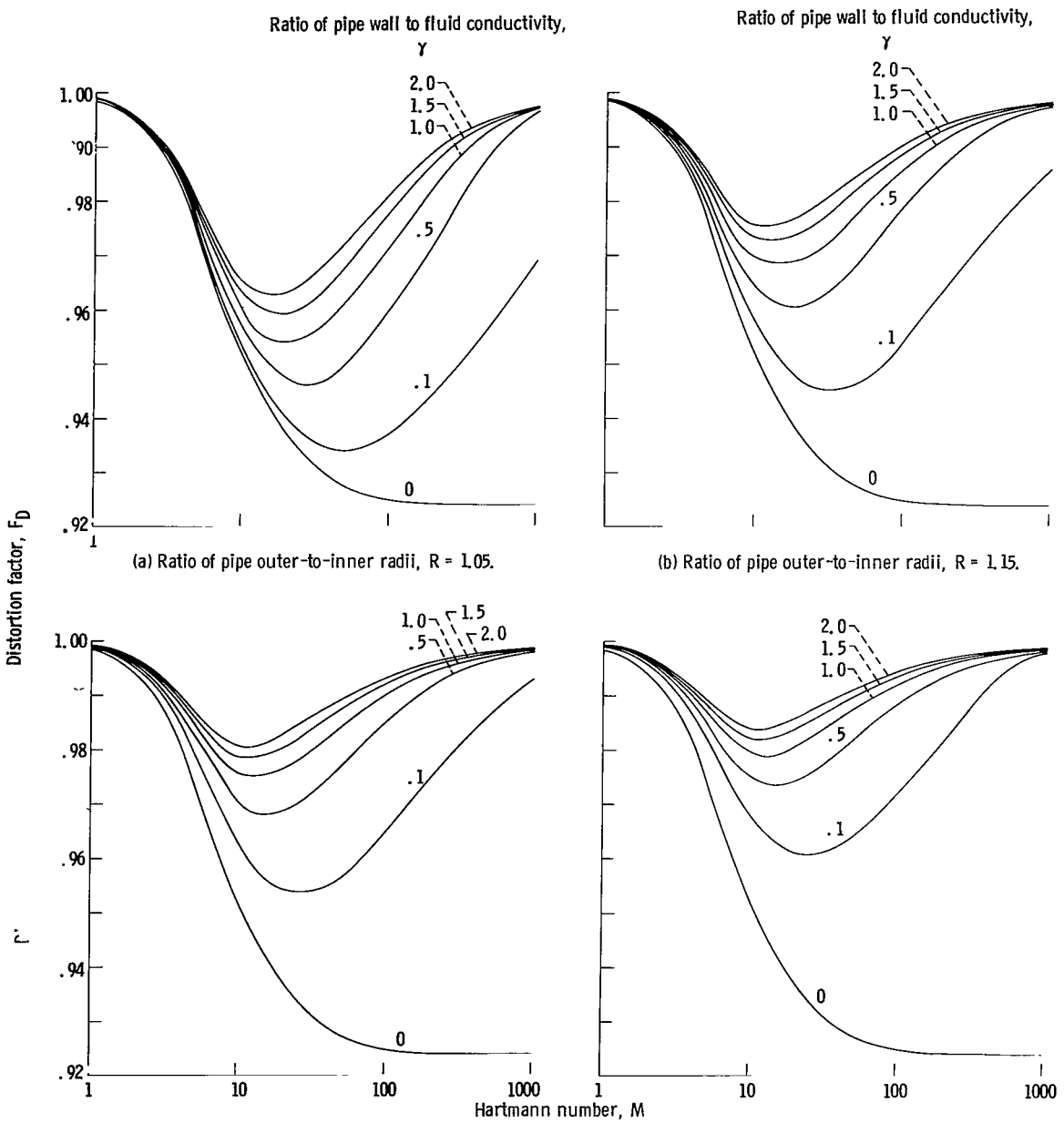

Figure 5. - Flowmeter distortion factor.

repeated for new values for R and γ of interest at the same M. The new guess used in step (1) was the solution for the previous R and γ.

Once the stationary point for F and the values of the adjustable parameters at the stationary point were computed, the approximate solutions for V and W could be determined by combining equations (32a), (32b), (34a), (34b), and (36a).

Numerical results. - Numerical results obtained using the variational principle and the Ritz technique are presented in table III. Values are given for the average velocity V_m/P_o, the induced potential difference W_{AD}/P_o, flowmeter sensitivity S, and distortion factor F_D for M values (1, 2, 5, 10, 20, 50, 100, 200, 500, and 1000), R values (1.00, 1.05, 1.15, 1.25, and 1.35), and γ values (0, 0.1, 0.5, 1.0, 1.5, and 2.0). The results for the distortion factor F_D are also presented in figures 5(a) to (d).

At low values of M, the distortion factor decreases with increasing M. The rate of decrease is greatest for pipes with a thin, poorly conducting wall and least for pipes with a thick, highly conductive wall. These results are in exact agreement with those found previously from the exact series solution. As M continues to increase, however, the distortion factor reaches a minimum if the pipe wall is conductive, and then it begins to increase and to asymptotically approach 1 as M becomes infinite. If the pipe wall is nonconductive, the distortion factor continues to decrease with increasing M and approaches approximately 0.924 as M becomes infinite.

The results in figure 5 show that it is important to include the effects of velocity profile distortion by the flowmeter itself when making precision flow measurements. If these effects are not considered, the indicated flow measurement will be less than the actual flow. If the pipe wall is nonconductive, this error increases with increasing M and approaches $(1 - 0.924/0.924)\times100$ or 8.2 percent as M becomes infinite. If the pipe wall is conductive, the error reaches a maximum, typically 2 to 5 percent, in the Hartmann number range 10 to 50 and then decreases to zero as M becomes infinite.

The reason for the behavior of F_D with increasing M can be seen by examining the velocity profiles. Figures 6 to 8 show the variation of V with ρ at fixed θ values of 0^o, 30^o, 60^o, and 90^o. The velocity is normalized with respect to V_c, the dimensionless velocity at the center of the pipe. Three cases are shown - the nonconducting pipe wall (R = 1.00, γ = 0), a thin, poorly conducting pipe wall (R = 1.05, γ = 0.1), and a thick, highly conducting pipe wall (R = 1.35, γ = 2.0).

At M = 0, the velocity profile is axially symmetric and assumes the normal Poiseuille shape for all cases. As M increases, the velocity profile becomes flattened particularly along $\theta = 0^o$. As M continues to increase, the profile also flattens along $\theta = 90^o$ if the pipe wall is conductive, and the profile eventually approaches slug flow as M becomes infinite. If the pipe wall is nonconductive, however, the flattening effect is not as pronounced along $\theta = 90^o$, and the profile does not approach slug flow as M becomes infinite.

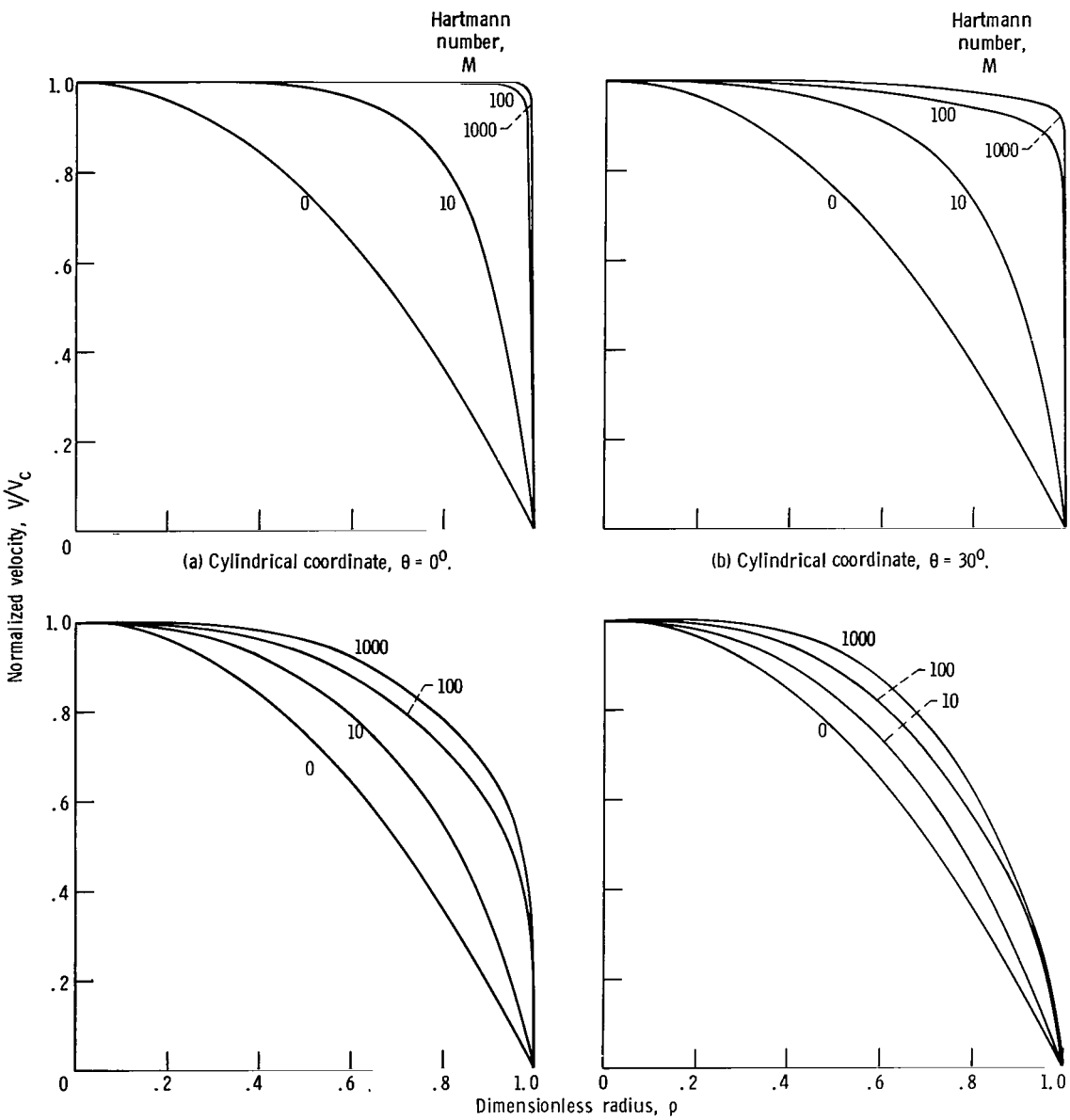

Figure 6. - Velocity profile. Ratio of pipe outer-to-inner radii, R = 1.00; ratio of pipe wall to fluid conductivity, γ = 0.

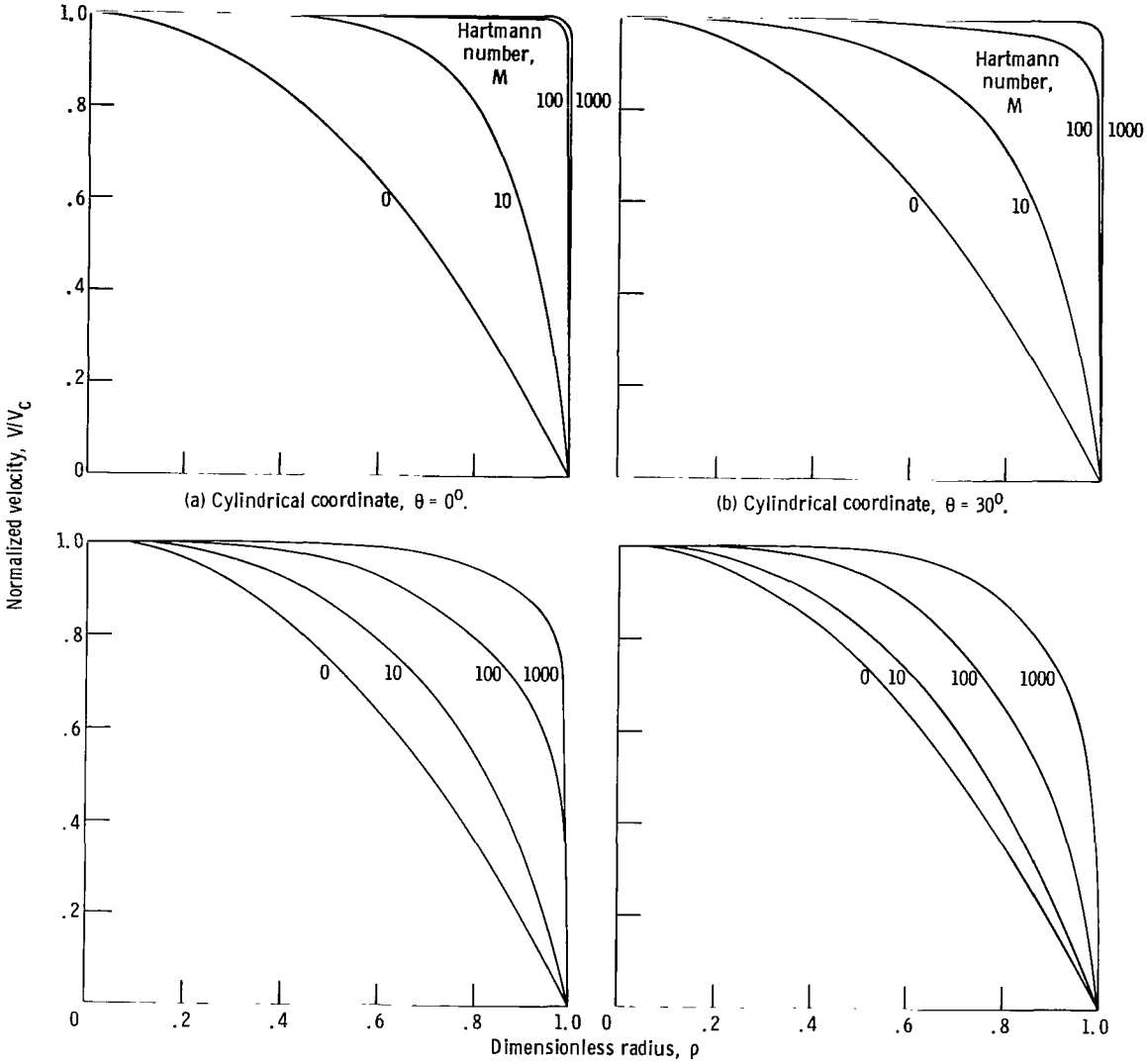

Figure 7. - Velocity profile. Ratio of pipe outer-to-inner radii, R = 1.05; ratio of pipe wall to fluid conductivity, γ = 0.1.

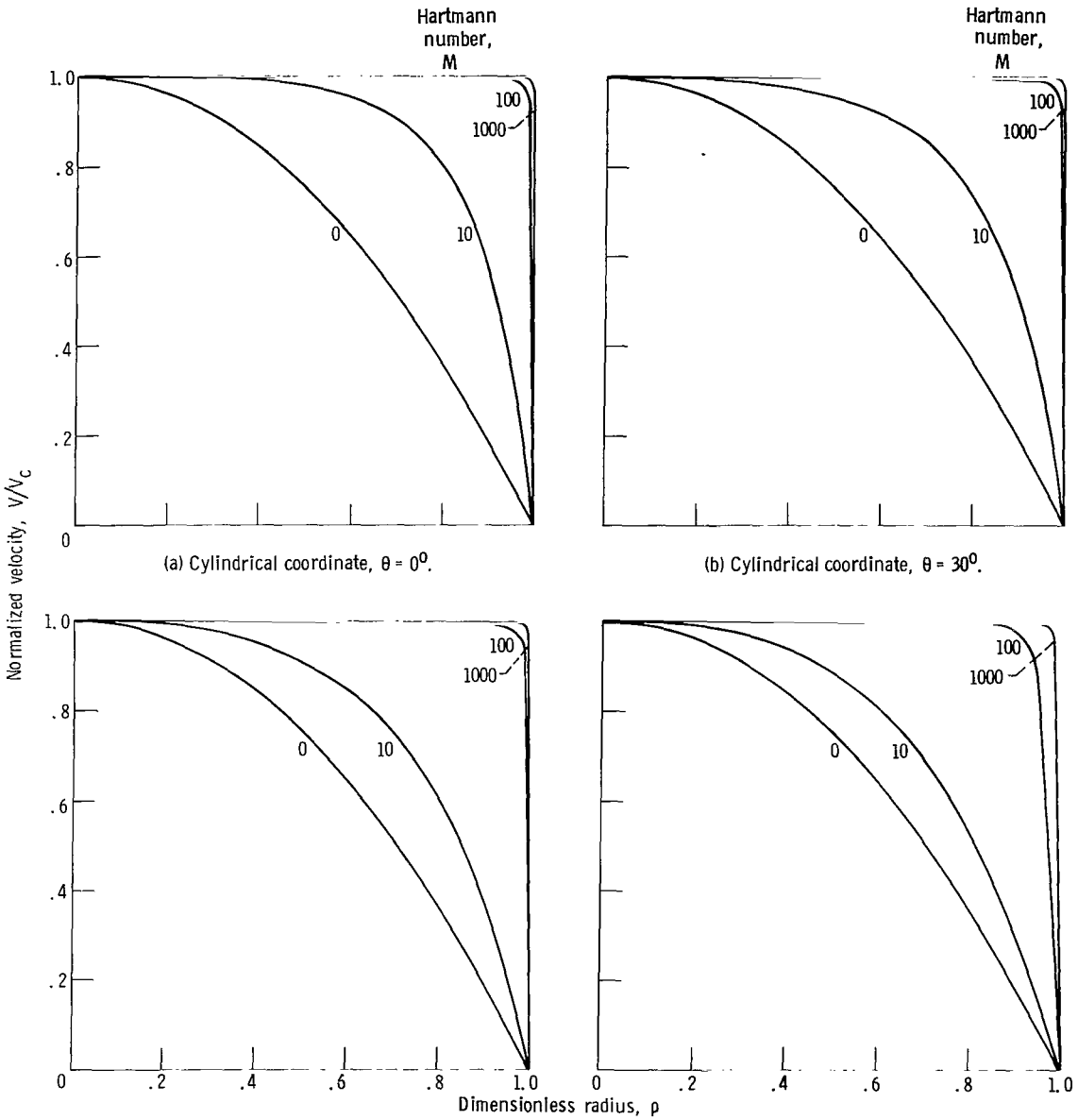

Figure 8. - Velocity profile. Ratio of pipe outer-to-inner radii, R = 1.35; ratio of pipe wall to fluid conductivity, γ = 2.0.

The reason for this flattening phenomenon is as follows. If the pipe wall is nonconductive, all the induced current must remain in the fluid since the current must form a closed path and there can be no current in the pipe wall. The net electromagnetic $\vec{J} \times \vec{B}$ force on the fluid is, thus, zero. Since $\vec{J} \times \vec{B}$ is not identically zero everywhere, the effect of this force is to distort the profile. The magnitude of this force is greatest near the center of the pipe where it opposes the flow and along the pipe wall near $\theta = 0^{\circ}$ and 180° where it aids the flow. This force is minimal near the pipe wall at $\theta = 90^{\circ}$ and 270° since $\vec{J}$ and $\vec{B}$ are essentially parallel in this region.

If the pipe wall is conductive, a fraction of the induced current in the fluid returns through the pipe wall. It was found that this fraction increases as M increases so that at high M virtually all the return current is in the pipe wall. In addition, it was found that the current density in the fluid becomes uniform over the cross section at high M giving a uniform electromagnetic force. The net effect is that the uniform electromagnetic and pressure forces balance each other in the core region resulting in a constant core velocity with negligible viscous forces. The viscous forces are only important in the thin boundary layer region where the velocity drops sharply from its core value to zero at the wall.

The reason for the variation of the distortion factor with M is now clear. If M is small, the distortion factor decreases with increasing M since the velocity profile becomes distorted because of the nonsymmetric electromagnetic forces. The distortion factor decreases rather than increases since the flow is being shifted from a region where the sensitivity weighting factor is high (along $\theta = 90^{\circ}$, 270°) to where it is low (along $\theta = 0^{\circ}$, 180°) (see figs. 3 and 4). As M continues to increase, the velocity profile goes to slug flow if the pipe wall is conductive, and thus the profile returns to axial symmetry. This causes the distortion factor to return to 1. If the pipe wall is nonconductive, the profile remains distorted from axial symmetry as M increases. The distortion factor for this case approaches 0.924 as M becomes infinite.

Accuracy of results. - The last main consideration is to determine the accuracy of the numerical results just presented. In most applications of the Ritz technique, the number of adjustable parameters is increased until the stationary value of the functional converges to a definite value. If the trial functions are expressed using a complete set of functions, convergence to the correct result is assured barring any error that may be introduced in the computation process. It is often difficult, however, to determine if convergence has actually been obtained without using many more parameters than are actually needed to obtain acceptably accurate results. In the problem under study, it was not possible because of computer time limitations to increase the number of adjustable parameters much beyond the point of apparent convergence. Thus, auxiliary tests must be used to check the results.

Numerical results from the exact series solution given in table I can be compared

with the variational solution results in table III for M values of 1, 2, 5, 10, and 20. The differences between these results are at most 1 part in the third place. To obtain a better feel for the magnitude of the error, the percentage difference between the exact and variational solutions is shown in figure 9 as a function of $(R - 1)\gamma$ at $M = 10$. The differences are determined for the average fluid velocity, induced potential difference, and center velocity. Figure 9 is based on results computed to 5 places which were later rounded to 3 places for presentation in tables I and III.

The figure shows that the center velocity has the largest error and the average velocity has the least error. In fact, the error in the average velocity is lower by more than an order of magnitude from the error in the center velocity. This phenomenon was expected since the stationary value of a functional, which in this case is proportional to the average velocity, is typically an order of magnitude more accurate than the error in the trial functions. The error in the induced potential difference W_{AD} also turns out to be about an order of magnitude less than the error in center velocity. Thus, the error in the

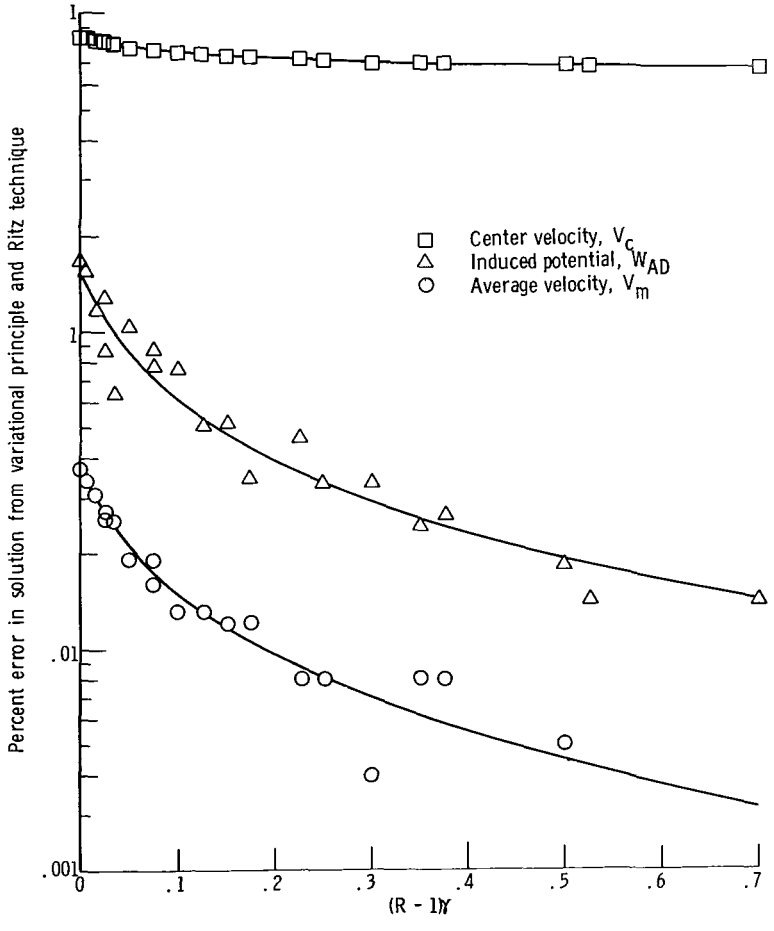

Figure 9. - Error in solution from variational principle and Ritz technique at Hartmann number M = 10.

flowmeter sensitivity and distortion factor is about an order of magnitude less than the error in the center velocity. The same relations between the various errors were also found for results at M values of 1, 2, and 5 although the magnitude of the errors decreased as M decreased.

Figure 9 also shows that the errors decrease as $(R - 1)\gamma$ increases. Thus, the nonconductive pipe wall gives the largest error, and the thickest most highly conductive pipe wall gives the least error. This phenomenon was also expected since it took the largest number of parameters to obtain convergence for the case of a nonconductive pipe wall. The same number of parameters required for convergence at a given M value for the nonconductive wall case were used for all conductive wall cases at the same value for M. Consequently, the accuracy of the results should improve as the quantity $(R - 1)\gamma$ increases.

The error in the results for higher M values can be estimated by assuming that the effects observed for low M are also true for high M (i.e., the errors in sensitivity and distortion factor are about an order of magnitude less than the error in center velocity and that a nonconductive pipe wall gives the largest error).

The center velocity for the nonconductive pipe wall case is the only quantity that can be easily computed exactly at any value of M. It is given by (eq. (21a) with $\rho = 0$)

$$V_c = \frac{P_o}{M} \frac{I_1\left(\frac{M}{2}\right)}{I_0\left(\frac{M}{2}\right)} \tag{37}$$

Figure 10 shows the percentage error in the variational solution for the dimension-

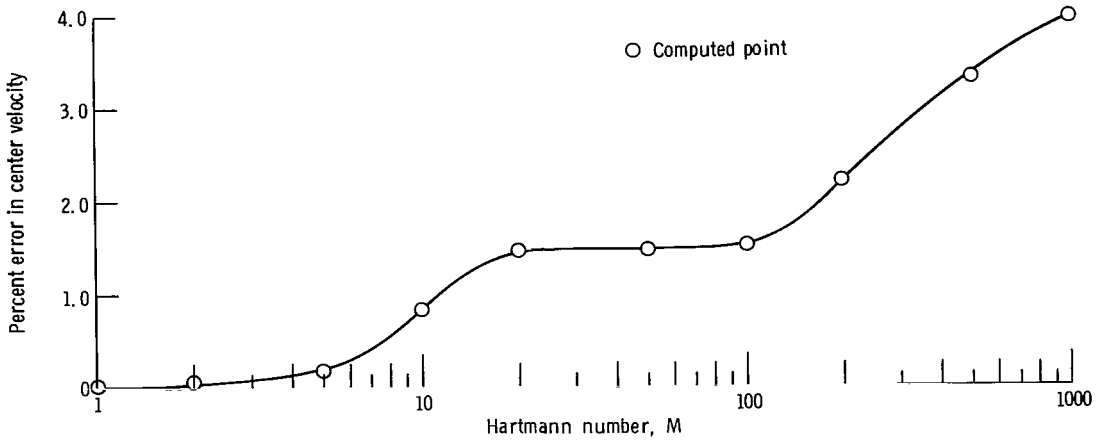

Figure 10. - Error in solution for center velocity for a nonconductive pipe wall (solution obtained using variational principle and Ritz technique).

less center velocity with a nonconductive pipe wall as a function of M. As shown, the error increases with increasing M and is slightly less than 4 percent at M = 1000. The flattening effect in the error curve at M values of 20 to 100 is due to the large increase that was made in the number of adjustable parameters at these M values (see table II) If the error relations observed at low M are valid for high M, the error in flowmeter sensitivity and distortion factor should be about 0.4 percent at M = 1000 for a nonconductive pipe wall and decrease from this value as M decreases and $(R - 1)\gamma$ increases.

Other checks on the results can be made at high M. It is known from the general theory of magnetohydrodynamic channel flow that if the channel wall is conductive, the velocity profile is constant over the channel cross section almost up to the wall where it drops rapidly to zero (refs. 13 and 14). Thus, the distortion factor for the circular channel under consideration should approach 1 as M becomes large which is in agreement with the computed results.

If the channel wall is nonconductive, the velocity profile remains distorted as M becomes large. Although all the mathematical steps can not be formally justified, it has been shown by Shercliff (ref. 13) and Gold (ref. 9) that the flowmeter sensitivity and distortion factor are asymptotic to $3\pi^2/32$ or 0.925 at high M. This value differs from the computed value of 0.924 at M = 1000 by only 0.16 percent.

Another possible way of checking the results is to examine the energy balance. The rate at which energy is being supplied to the moving fluid by the pressure source should equal the rate at which energy is being dissipated because of viscous losses in the fluid and ohmic losses in the fluid and wall. However, it can be shown that trial functions of the form given by equations (32) and (34) result in solutions which satisfy the energy balance equation exactly so that this check is not an independent test.

The approximate solutions can be tested, however, by determining how well they satisfy the basic equations (8a) to (8g). It is only necessary to examine equations (8a), (8b), and (8f) since the trial functions were selected to satisfy the remaining equations identically. The residuals, or differences between the left and right sides of these equations were computed at selected points over the pipe cross section $\rho \leq 1$ for equations (8a) and (8b) and along the fluid - pipe wall interface $\rho = 1$ for equation (8f).

For low values of M, it was found that if the residuals were small everywhere, then the approximate solution was almost exact as should be expected. Even if the residuals became large, however, which occasionally occurred near $\rho = 1$ for equation (8b), the approximate solution was still quite accurate. It was also observed that the residuals at all values of M became smaller as $(R - 1)\gamma$ increased which indicates that the error at all values of M is reduced as $(R - 1)\gamma$ is increased.

Rather than attempt to determine a relation between the size of the residuals and the error in the solution, which is a very difficult task, it was decided to test the solutions as follows. Using the approximate solution for the velocity, the potential was computed

by solving equations (8a), (8c), (8e), (8f), and (8g) exactly. The potential difference W_{AD} for this solution was then compared with that obtained directly from the variational solution. It was found that for M values of 20 or less the two solutions differed at most by 0.01 percent. For M values of 50 to 1000 the two solutions differed typically by 0.05 percent and at most by 0.15 percent.

The values shown in table III for the potential W_{AD}/P_0, flowmeter sensitivity, and distortion factor were actually computed by solving for the potential exactly using the approximate variational solution for the velocity. The difference between the solutions obtained this way and those obtained directly from the variational solution, however, are at most 2 parts in the third place.

The same procedure was also applied to equations (8b) and (8d) by solving them exactly for V using the approximate solution for W. The difference between the average value of this solution for V and the average found from the stationary value of the functional was at most a few parts in the fifth place.

As a final test, the method of solution using the Ritz technique was amended so that the trial functions for W exactly satisfied equations (8a), (8c), (8e), (8f), and (8g) for any given trial function for V. The advantage of this method is that for any choice for the trial function for V, the trial function for W is constrained so as to satisfy all the basic equations identically except for equation (8b). Thus, all the adjustable parameters can be concentrated in the trial function for V. The sole purpose of the variational principle and Ritz technique then reduces to generating the best approximate solution for equation (8b). This method of solution required a considerable amount of computer time so that it only was used for spot checking. The results obtained by this method differed very little from those given previously, however, indicating that the previous values are quite accurate. For example, at $M = 200$, $R = 1.00$, and $\gamma = 0$ the previous solution for the center velocity which was in error by 2.2 percent was reduced to 1.6 percent using this amended technique and 26 adjustable parameters compared with 40 parameters used previously (see table II). The corresponding changes in average velocity, output potential, flowmeter sensitivity, and distortion factor were 0.07, 0.16, 0.09, and 0.09 percent, respectively.

On the basis of all these tests it is felt that the error in the main quantities of interest, namely the flowmeter sensitivity and distortion factor, are of the order of a few tenths of a percent at the higher Hartmann numbers which are commonly found in liquid metal applications. This error is comparable to the error in determining the pipe shunting factor. Since the uncertainty in the electrical conductivity for most of the liquid metals is of the order of ±1 percent, the pipe shunting factor can only be determined typically to within ±0.25 percent. In addition, there are the errors associated with measuring the applied static magnetic field and output potential. However, these errors can often be held to less than ±0.1 percent.

CONCLUDING REMARKS

The theory of circular, transverse-field electromagnetic flowmeters has been extended to include the effects of distortion from axial symmetry in the fluid velocity profile. A general formulation was developed to relate the flowmeter sensitivity to any given but arbitrary velocity profile. It was found that flowmeters with a thick, highly conductive wall are the least sensitive to uncertainties in the velocity profile. The analysis was then extended to determine the effect of velocity profile distortion by the flowmeter itself. The fully developed profile was computed using a variational principle and the Ritz technique. It was found that if the distortion from axial symmetry in the fully developed profile were not considered in computing the flowmeter sensitivity, then errors of up to 8.2 percent would result in the flow measurement if the pipe wall were nonconductive. The error is reduced if the pipe wall is conductive, but it is still typically 2 to 5 percent for most liquid metal applications.

Lewis Research Center,
National Aeronautics and Space Administration,
Cleveland, Ohio, April 28, 1971,
120-27.

APPENDIX A

SYMBOLS

A_n	expansion coefficient in series for f (eq. (20a))
A_{ni}	expansion coefficient in trial function for f_n (eq. (34a))
a	pipe inner radius
$\hat{a}_r, \hat{a}_\theta, \hat{a}_z$	unit vectors
B	dimensionless induced magnetic field (= B_z/B_o)
$\vec{B}$	magnetic field
B_n	expansion coefficient in series for g (eq. (20b))
B_o	magnitude of $\vec{B}_o$
$\vec{B}_o$	applied uniform static magnetic field
B_z	induced axial magnetic field
b	outer radius of pipe
C_n	expansion coefficient for W in pipe wall (eq. (21c))
C_{nj}	expansion coefficient in trial function for g_n (eq. (34b))
$\vec{E}$	electric field
F	functional for MHD flow (eq. (30))
F_D	flowmeter distortion factor (eq. (29))
F_{st}	stationary value of F
f	auxiliary function (eqs. (18a) and (18b))
f_n	radial function in expansion for V (eq. (32a))
G	Green's function
G_n	radial function in expansion for G (eq. (12a))
g	auxiliary function (eqs. (18a) and (18b))
g_n	radial function in expansion for W (eq. (32b))
I_n	number of radial terms in n^{th} angular term in expansion for V (eq. (34a))
$\vec{J}$	electric current density
J_n	number of radial terms in n^{th} angular term in expansion for W (eq. (34b))

K	flowmeter weighting factor
L	entry length
M	Hartmann number ($= B_o a(\sigma_f/\eta)^{1/2}$)
N	number of angular terms
P_o	dimensionless axial pressure gradient $\left(=\frac{-a^2}{\eta V_o}\frac{\partial p}{\partial z}\right)$
p	pressure in fluid
R	ratio of pipe outer-to-inner radii ($= b/a$)
R_m	magnetic Reynolds number ($= \mu_o \sigma_f a V_o$)
Re	Reynolds number ($= \rho_m a V_o/\eta$)
Re_{crit}	critical Reynolds number
r, θ, z	cylindrical coordinates (fig. 2)
S	flowmeter sensitivity ($= U_{AD}/2aB_oV_{zm} = W_{AD}/2V_m$)
S_{nk}	infinite series (eq. (23f))
T_n	infinite series (eq. (23e))
U	induced potential
U_{AD}, U_{BC}	induced potential difference between points A-D or B-C (fig. 2)
V	dimensionless axial velocity ($= V_z/V_o$)
$\vec{V}$	fluid velocity
V_c	dimensionless center velocity
V_m	dimensionless average velocity
V_o	characteristic fluid velocity
V_z	axial fluid velocity
V_{zm}	average velocity
W	dimensionless induced potential ($= U/B_oaV_o$)
W_{AD}, W_{BC}	dimensionless potential difference between points A-D or B-C (fig. 2)
x, y, z	rectangular coordinates (fig. 2)
α_{ni}	exponent in expansion for f_n (eq. (34a))
β_{nj}	exponent in expansion for g_n (eq. (34b))
γ	ratio of wall to fluid conductivity ($= \sigma_w/\sigma_f$)

δ_{ij}	Kroniker delta function (= 1 if i = j, = 0 if $i \neq j$)
ϵ_n	(= 2 if n = 0, = 1 if $n \neq 0$)
ϵ_o	electric permittivity of free space
η	fluid viscosity
μ_o	magnetic permeability of free space
ρ	dimensionless radius (= r/a)
ρ_e	electric charge density
ρ_m	mass density of fluid
σ_f	electrical conductivity of fluid
σ_w	electrical conductivity of pipe wall
$\Omega_1, \ldots, \Omega_n$	adjustable prameters

APPENDIX B

FLOWMETER PARAMETERS

The purpose of this section is to acquaint the reader with some typical values for the flowmeter parameters that are encountered in liquid metal applications. First, consider the ratio of outer-to-inner pipe radii R. Figure 11 shows R as a function of the pipe

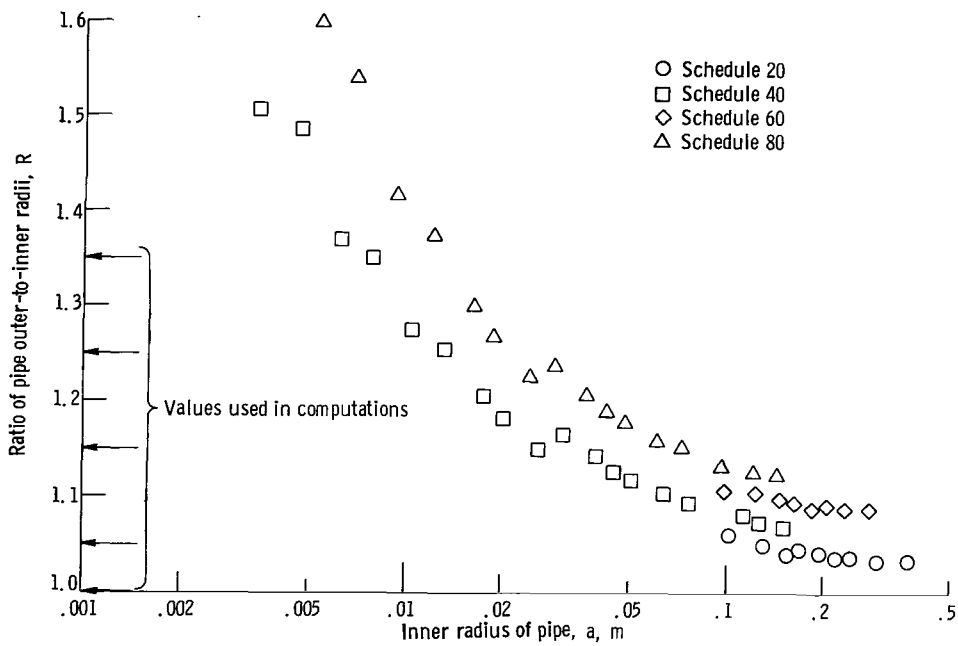

Figure 11. - Ratio of outer-to-inner radii for commercial steel pipes.

inner radius a for schedule 20, 40, 60, and 80 commercial steel pipes. Despite the large variation in diameters and wall thicknesses for these pipes, the points on the curve R against a fall within a narrow band. Because of the large number of applications for pipes in the inner radius range 0.01 to 0.1 meter, the R values used in the computations were concentrated in the corresponding range of 1.00 to 1.35. In addition to the various schedule pipes, tubing is frequently used in liquid metal applications; particularly thin wall tubing in proposed space applications where weight is an important factor. The R values for this tubing are generally in the range 1.02 to 1.10.

Next, consider the ratio of the pipe wall to fluid electrical conductivity γ. Figure 12 shows this ratio as a function of temperature for liquid mercury, lithium, sodium, potassium, and NaK for pipe walls made of 316 stainless steel and T_{111}, a tantalum base

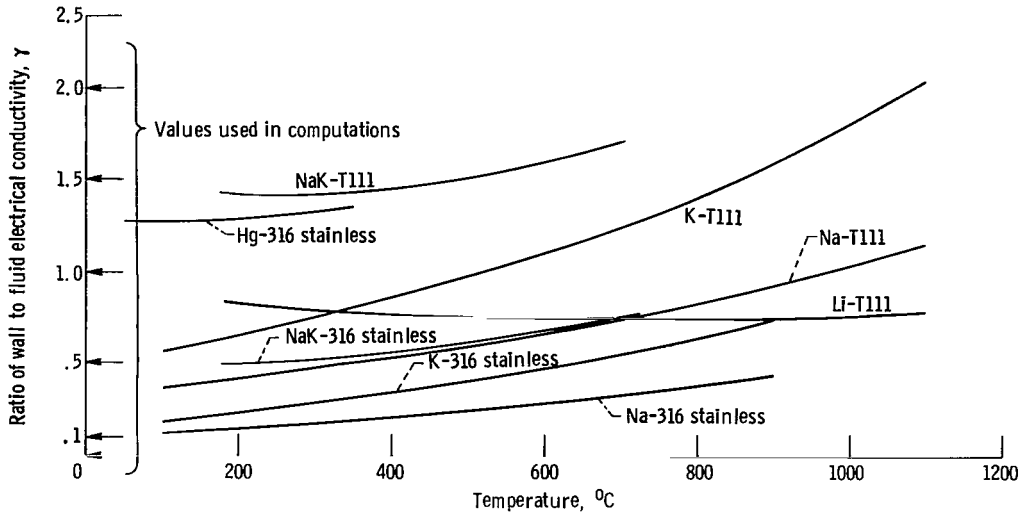

Figure 12. - Ratio of wall to fluid electrical conductivity for common liquid metals and pipe materials.

alloy. The conductivities of the liquid metals were obtained from references 23 and 24 and the conductivities of the pipe wall materials were obtained from references 25 and 26. As shown in figure 12, the values of γ encountered in practice are rather uniformly distributed over the range 0 to 2.

REFERENCES

1. Williams, E. J.: The Induction of Electromotive Forces in a Moving Liquid by a Magnetic Field, and its Application to an Investigation of the Flow of Liquids. Proc. Phys. Soc. (London), vol. 42, pt. 5, no. 235, Aug. 15, 1930, pp. 466-478.

2. Thürlemann, B.: Methode zur elektrischen Geschwindigkeitsmessung von Flüssigkeiten. Helv. Phys. Acta, vol. 14, 1941, pp. 383-417.

3. Kolin, Alexander: An Alternating Field Induction Flow Meter of High Sensitivity. Rev. Sci. Inst., vol. 16, no. 5, May 1945, pp. 109-116.

4. Elrod, H. G., Jr.; and Fouse, R. R.: An Investigation of Electromagnetic Flowmeters. Trans. ASME, vol. 74, no. 4, May 1952, pp. 589-594.

5. Shercliff, J. A.: Relation Between the Velocity Profile and the Sensitivity of Electromagnetic Flowmeters. J. Appl. Phys., vol. 25, no. 6, June 1954, pp. 817-818.

6. Shercliff, J. A.: The Theory of Electromagnetic Flow-Measurement. Cambridge University Press, 1962.

7. Uflyand, Ya. S.: Hartmann Problem for a Circular Tube. Soviet Phys.-Tech. Phys., vol. 5, no. 10, Apr. 1961, pp. 1194-1196.

8. Uhlenbusch, J.; and Fischer, E.: Hydromagnetische Strömung im kreiszylindrischen Rohr. Zeit. f. Physik, vol. 164, Aug. 3, 1961, pp. 190-198.

9. Gold, Richard R.: Magnetohydrodynamic Pipe Flow. Part 1. J. Fluid Mech., vol. 13, pt. 4, Aug. 1962, pp. 505-512.

10. Singh, S. N.; and Nariboli, G. A.: Asymptotic Solution for the Hartmann Problem Through Circular Tube. Appl. Sci. Res., Sec. B, vol. 11, 1964, pp. 145-160.

11. Shercliff. J. A.: The Theory of the D. C. Electromagnetic Flowmeter for Liquid Metals. Rep. AERE-X/R-1052, Atomic Energy Research Establishment, Nov. 1952.

12. Ihara, Sadatoshi; Tajima, Kiyohiro; and Matsushima, Akira: The Flow of Conducting Fluids in Circular Pipes with Finite Conductivity Under Uniform Transverse Magnetic Fluids. J. Appl. Mech., vol. 34, no. 1, Mar. 1967, pp. 29-36.

13. Shercliff, J. A.: The Flow of Conducting Fluids in Circular Pipes Under Transverse Magnetic Fields. J. Fluid Mech., vol. 1, pt. 6, Dec. 1956, pp. 644-666.

14. Chang, Chieh C.; and Lundgren, Thomas S.: Duct Flow in Magnetohydrodynamics. Zeit. f. Angew. Math. Mech., vol. 12, 1961, pp. 100-114.

15. Gold, Richard R.: Effect of Wall Conductance on Magnetohydrodynamic Flow Through Finite Cross-Section Channels. AIAA J., vol. 5, no. 3, Mar. 1967, pp. 539-544.

16. Wenger, Norman C.: A Variational Principle for Magnetohydrodynamic Channel Flow. NASA TN D-5591, 1969.

17. Wenger, Norman C.: A Variational Principle for Magnetohydrodynamic Channel Flow. J. Fluid Mech., vol. 43, pt. 1, Aug. 17, 1970, pp. 211-224.

18. Shercliff, J. A.: Entry of Conducting and Non-Conducting Fluids in Pipes. Proc. Camb. Phil. Soc., vol. 52, pt. 3, July 1956, pp. 573-583.

19. Loeffler, A. L., Jr.; Maciulaitis, A.; and Hoff, M.: Circular Channel Magnetohydrodynamic Experiments in a Transverse Magnetic Field. Phys. Fluids, vol. 12, no. 11, Nov. 1969, pp. 2445-2447.

20. Hunt, J. C. R.: A Uniqueness Theorem for Magnetohydrodynamic Duct Flows. Proc. Camb. Phil. Soc., vol. 65. no. 1, Jan 1969, pp. 319-327.

21. Powell, M. J. D.: An Efficient Method for Finding the Minimum of a Function of Several Variables Without Calculating Derivatives. Computer J., vol. 7, no. 2, July 1964, pp. 155-162.

22. Powell, M. J. D.: A Fortran Subroutine for Solving Systems of Non-Linear Algebraic Equations. Rep. AERE-R-5947, Atomic Energy Research Establishment, Nov. 1968.

23. Weatherford, W. D., Jr.; Tyler, John C.; and Ku, P. M.: Properties of Inorganic Energy-Conversion and Heat-Transfer Fluids for Space Applications. Southwest Research Inst. (WADD TR 61-96), Nov. 1961.

24. Achener, P. Y.; Mackewicz, W. V.; Fisher, D. L.; and Camp, D. C.· Thermophysical and Heat Transfer Properties of Alkali Metals. Rep. AGN-8195, vol. 1, Aerojet-General Nucleonics, Apr. 1968.

25. Verkamp, J. P.; and Rhudy, R. G.: Electromagnetic Alkali Metal Pump Research Program. NASA CR-380, 1966.

26. Kueser, P. E.; Toth, J. W.; and McRae, R. C.: Bore Seal Technology Topical Report. Rep. WAED-64.54E, Westinghouse Electric Corp. (NASA CR-54093), Dec. 1964.

TABLE I. - RESULTS FROM EXACT SERIES SOLUTION

(a) Hartmann number, M = 1

Pipe outer-to-inner radii ratio, R	Pipe wall to fluid conductivity ratio, γ					
	0	0.1	0.5	1.0	1.5	2.0
	Average velocity, V_m/P_o					
1.00	1.22×10^{-1}	---	---	---	---	---
1.05	---	1.22×10^{-1}	1.22×10^{-1}	1.22×10^{-1}	1.21×10^{-1}	1.21×10^{-1}
1.15	---	↓	1.22	1.21	1.20	1.19
1.25	---		1.21	1.20	1.19	1.18
1.35	---		1.21	1.19	1.18	1.17
	Induced potential, W_{AD}/P_o					
1.00	2.45×10^{-1}	---	---	---	---	---
1.05	---	2.43×10^{-1}	2.38×10^{-1}	2.32×10^{-1}	2.26×10^{-1}	2.20×10^{-1}
1.15	---	2.39	2.25	2.10	1.96	1.85
1.25	---	2.33	2.13	1.92	1.74	1.60
1.35	---	2.27	2.01	1.76	1.57	1.42
	Sensitivity, S					
1.00	0.998	-----	-----	-----	-----	-----
1.05	---	0.992	0.973	0.951	0.929	0.909
1.15	---	.975	.925	.868	.819	.774
1.25	---	.953	.878	.799	.733	.677
1.35	---	.928	.834	.740	.665	.604
	Distortion factor, F_D					
1.00	0.998	-----	-----	-----	-----	-----
1.05	---	0.998	0.998	0.998	0.999	0.999
1.15	---	.998	.999	.999	↓	↓
1.25	---	.999	.999	.999		
1.35	---	.999	.999	.999		

TABLE I. - Continued. RESULTS FROM EXACT SERIES SOLUTION

(b) Hartmann number, M = 2

Pipe outer-to-inner radii ratio, R	Pipe wall to fluid conductivity ratio, γ					
	0	0.1	0.5	1.0	1.5	2.0
	Average velocity, V_m/P_o					
1.00	1.16×10^{-1}	---	---	---	---	---
1.05	---	1.16×10^{-1}	1.15×10^{-1}	1.13×10^{-1}	1.12×10^{-1}	1.11×10^{-1}
1.15	---	1.15	1.13	1.10	1.07	1.05
1.25	---	1.15	1.11	1.07	1.04	1.02
1.35	---	1.14	1.09	1.05	1.02	9.90×10^{-2}
	Induced potential, W_{AD}/P_o					
1.00	2.30×10^{-1}	---	---	---	---	---
1.05	---	2.28×10^{-1}	2.22×10^{-1}	2.15×10^{-1}	2.08×10^{-1}	2.02×10^{-1}
1.15	---	2.24	2.07	1.90	1.75	1.63
1.25	---	2.18	1.94	1.70	1.52	1.37
1.35	---	2.12	1.82	1.55	1.35	1.19
	Sensitivity, S					
1.00	0.994	-----	-----	-----	-----	-----
1.05	---	0.988	0.969	0.947	0.926	0.905
1.15	---	.971	.921	.866	.816	.772
1.25	---	.950	.875	.797	.731	.676
1.35	---	.925	.832	.738	.664	.603
	Distortion factor, F_D					
1.00	0.994	-----	-----	-----	-----	-----
1.05	---	0.994	0.994	0.994	0.995	0.995
1.15	---	.994	.995	.995	.996	.996
1.25	---	.995	.996	.996	.996	.997
1.35	---	.996	.996	.997	.997	.997

TABLE I. - Continued. RESULTS FROM EXACT SERIES SOLUTION

(c) Hartmann number, M = 5

Pipe outer-to-inner radii ratio, R	Pipe wall to fluid conductivity ratio, γ					
	0	0.1	0.5	1.0	1.5	2.0
	Average velocity, V_m/P_o					
1.00	8.96×10^{-2}	---	---	---	---	---
1.05	---	8.87×10^{-2}	8.51×10^{-2}	8.11×10^{-2}	7.77×10^{-2}	7.47×10^{-2}
1.15	---	8.69	7.82	7.03	6.46	6.02
1.25	---	8.55	7.33	6.38	5.76	5.32
1.35	---	8.43	6.97	5.95	5.32	4.90
	Induced potential, W_{AD}/P_o					
1.00	1.75×10^{-1}	---	---	---	---	---
1.05	---	1.72×10^{-1}	1.62×10^{-1}	1.51×10^{-1}	1.42×10^{-1}	1.33×10^{-1}
1.15	---	1.66	1.42	1.20	1.04	9.19×10^{-2}
1.25	---	1.60	1.27	1.01	8.33×10^{-2}	7.12
1.35	---	1.54	1.15	8.70×10^{-2}	7.00	5.86
	Sensitivity, S					
1.00	0.975	-----	-----	-----	-----	-----
1.05	---	0.969	0.952	0.931	0.911	0.892
1.15	---	.955	.907	.854	.806	.763
1.25	---	.935	.864	.788	.724	.669
1.35	---	.913	.823	.731	.658	.598
	Distortion factor, F_D					
1.00	0.975	-----	-----	-----	-----	-----
1.05	---	0.975	0.976	0.978	0.979	0.980
1.15	---	.977	.980	.982	.983	.985
1.25	---	.980	.983	.985	.986	.987
1.35	---	.982	.985	.987	.988	.989

TABLE I. - Continued. RESULTS FROM EXACT SERIES SOLUTION

(d) Hartmann number, M = 10

Pipe outer-to-inner radii ratio, R	Pipe wall to fluid conductivity ratio, γ					
	0	0.1	0.5	1.0	1.5	2.0
	Average velocity, V_m/P_o					
1.00	6.01×10^{-2}	---	---	---	---	---
1.05	---	5.84×10^{-2}	5.25×10^{-2}	4.68×10^{-2}	4.24×10^{-2}	3.90×10^{-2}
1.15	---	5.55	4.30	3.45	2.93	2.59
1.25	---	5.31	3.75	2.87	2.40	2.11
1.35	---	5.12	3.39	2.54	2.11	1.86
	Induced potential, W_{AD}/P_o					
1.00	1.15×10^{-1}	---	---	---	---	---
1.05	---	1.11×10^{-1}	9.80×10^{-2}	8.57×10^{-2}	7.61×10^{-2}	6.85×10^{-2}
1.15	---	1.04	7.69	5.82	4.68	3.92
1.25	---	9.77×10^{-2}	6.40	4.48	3.45	2.80
1.35	---	9.23	5.52	3.68	2.76	2.21
	Sensitivity, S					
1.00	0.954	-----	-----	-----	-----	-----
1.05	---	0.949	0.934	0.915	0.897	0.879
1.15	---	.936	.894	.844	.798	.756
1.25	---	.920	.853	.781	.718	.665
1.35	---	.900	.814	.726	.654	.595
	Distortion factor, F_D					
1.00	0.954	-----	-----	-----	-----	-----
1.05	---	0.955	0.958	0.961	0.964	0.966
1.15	---	.959	.965	.970	.974	.976
1.25	---	.964	.971	.976	.979	.981
1.35	---	.968	.975	.980	.982	.984

TABLE I. - Concluded. RESULTS FROM EXACT SERIES SOLUTION

(e) Hartmann number, M = 20

Pipe outer-to-inner radii ratio, R	Pipe wall to fluid conductivity ratio, γ					
	0	0.1	0.5	1.0	1.5	2.0
	Average velocity, V_m/P_o					
1.00	3.53×10^{-2}	---	---	---	---	---
1.05	---	3.30×10^{-2}	2.62×10^{-2}	2.11×10^{-2}	1.78×10^{-2}	1.55×10^{-2}
1.15	---	2.95	1.82	1.28	1.02	8.59×10^{-3}
1.25	---	2.69	1.46	9.87×10^{-3}	7.78×10^{-3}	6.60
1.35	---	2.51	1.25	8.36	6.61	5.65
	Induced potential, W_{AD}/P_o					
1.00	6.63×10^{-2}	---	---	---	---	---
1.05	---	6.17×10^{-2}	4.85×10^{-2}	3.84×10^{-2}	3.18×10^{-2}	2.71×10^{-2}
1.15	---	5.45	3.24	2.16	1.62	1.30
1.25	---	4.91	2.48	1.54	1.12	8.79×10^{-3}
1.35	---	4.48	2.03	1.21	8.66×10^{-3}	6.74
	Sensitivity, S					
1.00	0.938	-----	-----	-----	-----	-----
1.05	---	0.935	0.924	0.909	0.892	0.876
1.15	---	.925	.889	.842	.798	.757
1.25	---	.911	.851	.781	.719	.666
1.35	---	.893	.813	.726	.655	.596
	Distortion factor, F_D					
1.00	0.938	-----	-----	-----	-----	-----
1.05	---	0.941	0.948	0.954	0.959	0.963
1.15	---	.947	.960	.969	.974	.977
1.25	---	.955	.968	.976	.980	.982
1.35	---	.961	.974	.981	.984	.986

TABLE II. - NUMBER OF ADJUSTABLE PARAMETERS IN TRIAL FUNCTIONS FOR VELOCITY AND POTENTIAL

Hartmann number, M	Number of angular terms, N	Number of radial terms in each angular term							
		Velocity				Potential			
		I_1	I_2	I_3	I_4	J_1	J_2	J_3	J_4
1	2	3	2	-	-	3	2	-	-
2	2	3	2	-	-	3	2	-	-
5	2	3	2	-	-	3	2	-	-
10	2	3	2	-	-	3	2	-	-
20	2	3	2	-	-	3	2	-	-
50	4	4	2	3	3	3	2	2	-
100	4	4	3	3	3	3	2	2	-
200	4	4	3	3	3	3	2	2	-
500	4	4	3	3	3	3	2	2	-
1000	4	4	3	3	3	3	2	2	-

TABLE III. - RESULTS FROM VARIATIONAL PRINCIPLE AND RITZ TECHNIQUE

(a) Hartmann number, M = 1

Pipe outer-to-inner radii ratio, R	Pipe wall to fluid conductivity ratio, γ					
	0	0.1	0.5	1.0	1.5	2.0
	Average velocity, V_m/P_o					
1.00	1.22×10^{-1}	---	---	---	---	---
1.05	---	1.22×10^{-1}	1.22×10^{-1}	1.22×10^{-1}	1.21×10^{-1}	1.21×10^{-1}
1.15	---	1.22	1.22	1.21	1.20	1.19
1.25	---	1.22	1.21	1.20	1.19	1.18
1.35	---	1.22	1.21	1.19	1.18	1.17
	Induced potential, W_{AD}/P_o					
1.00	2.45×10^{-1}	---	---	---	---	---
1.05	---	2.43×10^{-1}	2.38×10^{-1}	2.32×10^{-1}	2.26×10^{-1}	2.20×10^{-1}
1.15	---	2.39	2.25	2.10	1.96	1.85
1.25	---	2.33	2.13	1.92	1.74	1.60
1.35	---	2.27	2.01	1.76	1.57	1.42
	Sensitivity, S					
1.00	0.998	-----	-----	-----	-----	-----
1.05	---	0.992	0.973	0.951	0.929	0.909
1.15	---	.975	.925	.868	.819	.774
1.25	---	.953	.878	.799	.733	.677
1.35	---	.928	.834	.740	.665	.604
	Distortion factor, F_D					
1.00	0.998	-----	-----	-----	-----	-----
1.05	---	0.998	0.998	0.998	0.999	0.999
1.15	---	.998	.999	.999	↓	↓
1.25	---	.999	.999	.999		
1.35	---	.999	.999	.999		

TABLE III. - Continued. RESULTS FROM VARIATIONAL PRINCIPLE AND RITZ TECHNIQUE

(b) Hartmann number, M = 2

Pipe outer-to-inner radii ratio, R	Pipe wall to fluid conductivity ratio, γ					
	0	0.1	0.5	1.0	1.5	2.0
	Average velocity, V_m/P_o					
1.00	1.16×10^{-1}	---	---	---	---	---
1.05	---	1.16×10^{-1}	1.15×10^{-1}	1.13×10^{-1}	1.12×10^{-1}	1.11×10^{-1}
1.15	---	1.15	1.13	1.10	1.07	1.05
1.25	---	1.15	1.11	1.07	1.04	1.02
1.35	---	1.14	1.09	1.05	1.02	9.90×10^{-2}
	Induced potential, W_{AD}/P_o					
1.00	2.30×10^{-1}	---	---	---	---	---
1.05	---	2.28×10^{-1}	2.22×10^{-1}	2.15×10^{-1}	2.08×10^{-1}	2.02×10^{-1}
1.15	---	2.24	2.07	1.90	1.75	1.63
1.25	---	2.18	1.94	1.70	1.52	1.37
1.35	---	2.12	1.82	1.55	1.35	1.19
	Sensitivity, S					
1.00	0.994	-----	-----	-----	-----	-----
1.05	---	0.988	0.969	0.947	0.926	0.905
1.15	---	.971	.921	.866	.816	.772
1.25	---	.950	.875	.797	.731	.676
1.35	---	.925	.832	.738	.664	.603
	Distortion factor, F_D					
1.00	0.994	-----	-----	-----	-----	-----
1.05	---	0.994	0.994	0.994	0.995	0.995
1.15	---	.994	.995	.995	.996	.996
1.25	---	.995	.996	.996	.996	.997
1.35	---	.996	.996	.997	.997	.997

TABLE III. - Continued. RESULTS FROM VARIATIONAL PRINCIPLE AND RITZ TECHNIQUE

(c) Hartmann number, M = 5

Pipe outer-to-inner radii ratio, R	Pipe wall to fluid conductivity ratio, γ					
	0	0.1	0.5	1.0	1.5	2.0
	Average velocity, V_m/P_o					
1.00	8.96×10^{-2}	---	---	---	---	---
1.05	---	8.86×10^{-2}	8.51×10^{-2}	8.11×10^{-2}	7.77×10^{-2}	7.47×10^{-2}
1.15	---	8.69	7.82	7.03	6.46	6.02
1.25	---	8.56	7.33	6.38	5.76	5.32
1.35	---	8.42	6.97	5.95	5.32	4.90
	Induced potential, W_{AD}/P_o					
1.00	1.75×10^{-1}	---	---	---	---	---
1.05	---	1.72×10^{-1}	1.62×10^{-1}	1.51×10^{-1}	1.42×10^{-1}	1.33×10^{-1}
1.15	---	1.66	1.42	1.20	1.04	9.19×10^{-2}
1.25	---	1.60	1.27	1.01	8.33×10^{-2}	7.12
1.35	---	1.54	1.15	8.69×10^{-2}	7.00	5.86
	Sensitivity, S					
1.00	0.974	-----	-----	-----	-----	-----
1.05	---	0.969	0.952	0.931	0.911	0.891
1.15	---	.954	.907	.854	.806	.763
1.25	---	.935	.864	.788	.724	.669
1.35	---	.913	.822	.731	.658	.598
	Distortion factor, F_D					
1.00	0.974	-----	-----	-----	-----	-----
1.05	---	0.975	0.976	0.977	0.978	0.979
1.15	---	.977	.979	.982	.983	.984
1.25	---	.980	.982	.985	.986	.987
1.35	---	.982	.985	.987	.988	.989

TABLE III. - Continued. RESULTS FROM VARIATIONAL PRINCIPLE AND RITZ TECHNIQUE

(d) Hartmann number, M = 10

Pipe outer-to-inner radii ratio, R	Pipe wall to fluid conductivity ratio, γ					
	0	0.1	0.5	1.0	1.5	2.0
	Average velocity, V_m/P_o					
1.00	6.01×10^{-2}	---	---	---	---	---
1.05	---	5.83×10^{-2}	5.24×10^{-2}	4.68×10^{-2}	4.24×10^{-2}	3.90×10^{-2}
1.15	---	5.54	4.30	3.45	2.93	2.59
1.25	---	5.31	3.75	2.87	2.40	2.11
1.35	---	5.12	3.39	2.54	2.11	1.86
	Induced potential, W_{AD}/P_o					
1.00	1.14×10^{-1}	---	---	---	---	---
1.05	---	1.11×10^{-1}	9.79×10^{-2}	8.56×10^{-2}	7.61×10^{-2}	6.85×10^{-2}
1.15	---	1.04	7.69	5.82	4.68	3.92
1.25	---	9.77×10^{-2}	6.40	4.48	3.45	2.80
1.35	---	9.22	5.52	3.68	2.76	2.21
	Sensitivity, S					
1.00	0.952	---	---	---	---	---
1.05	---	0.948	0.933	0.914	0.896	0.878
1.15	---	.936	.893	.843	.798	.756
1.25	---	.919	.853	.780	.718	.665
1.35	---	.900	.814	.726	.654	.595
	Distortion factor, F_D					
1.00	0.952	---	---	---	---	---
1.05	---	0.954	0.957	0.960	0.963	0.965
1.15	---	.958	.964	.970	.973	.976
1.25	---	.963	.970	.976	.979	.981
1.35	---	.968	.975	.980	.982	.984

TABLE III. - Continued. RESULTS FROM VARIATIONAL PRINCIPLE AND RITZ TECHNIQUE

(e) Hartmann number, M = 20

Pipe outer-to-inner radii ratio, R	Pipe wall to fluid conductivity ratio, γ					
	0	0.1	0.5	1.0	1.5	2.0
	Average velocity, V_m/P_o					
1.00	3.53×10^{-2}	---	---	---	---	---
1.05	---	3.30×10^{-2}	2.62×10^{-2}	2.11×10^{-2}	1.78×10^{-2}	1.55×10^{-2}
1.15	---	2.94	1.82	1.28	1.02	8.59×10^{-3}
1.25	---	2.69	1.46	9.87×10^{-3}	7.78×10^{-3}	6.60
1.35	---	2.51	1.25	8.36	6.61	5.65
	Induced potential, W_{AD}/P_o					
1.00	6.62×10^{-2}	---	---	---	---	---
1.05	---	6.17×10^{-2}	4.85×10^{-2}	3.84×10^{-2}	3.18×10^{-2}	2.71×10^{-2}
1.15	---	5.45	3.24	2.16	1.62	1.30
1.25	---	4.91	2.48	1.54	1.12	8.79×10^{-3}
1.35	---	4.48	2.03	1.21	8.66×10^{-3}	6.74
	Sensitivity, S					
1.00	0.937	-----	-----	-----	-----	-----
1.05	---	0.935	0.924	0.909	0.893	0.876
1.15	---	.925	.890	.843	.799	.758
1.25	---	.911	.852	.781	.720	.666
1.35	---	.893	.814	.727	.655	.596
	Distortion factor, F_D					
1.00	0.937	-----	-----	-----	-----	-----
1.05	---	0.940	0.948	0.954	0.959	0.963
1.15	---	.947	.961	.969	.974	.978
1.25	---	.955	.969	.976	.980	.983
1.35	---	.961	.974	.981	.984	.986

TABLE III. - Continued. RESULTS FROM VARIATIONAL PRINCIPLE AND RITZ TECHNIQUE

(f) Hartmann number, M = 50

Pipe outer-to-inner radii ratio, R	Pipe wall to fluid conductivity ratio, γ					
	0	0.1	0.5	1.0	1.5	2.0
	Average velocity, V_m/P_o					
1.00	1.57×10^{-2}	---	---	---	---	---
1.05	---	1.31×10^{-2}	8.01×10^{-3}	5.48×10^{-3}	4.22×10^{-3}	3.46×10^{-3}
1.15	---	1.01	4.37	2.69	2.01	1.64
1.25	---	8.41×10^{-3}	3.18	1.93	1.45	1.20
1.35	---	7.34	2.60	1.58	1.21	1.01
	Induced potential, W_{AD}/P_o					
1.00	2.91×10^{-2}	---	---	---	---	---
1.05	---	2.43×10^{-2}	1.48×10^{-2}	1.00×10^{-2}	7.60×10^{-3}	6.12×10^{-3}
1.15	---	1.87	7.84×10^{-3}	4.57×10^{-3}	3.23	2.50
1.25	---	1.54	5.47	3.04	2.11	1.61
1.35	---	1.32	4.26	2.31	1.59	1.21
	Sensitivity, S					
1.00	0.927	-----	-----	-----	-----	-----
1.05	---	0.928	0.926	0.915	0.901	0.885
1.15	---	.924	.897	.851	.805	.764
1.25	---	.913	.859	.787	.725	.671
1.35	---	.896	.820	.732	.659	.599
	Distortion factor, F_D					
1.00	0.927	-----	-----	-----	-----	-----
1.05	---	0.934	0.950	0.961	0.968	0.972
1.15	---	.946	.969	.978	.983	.985
1.25	---	.956	.977	.984	.987	.989
1.35	---	.964	.982	.988	.990	.991

TABLE III. - Continued. RESULTS FROM VARIATIONAL PRINCIPLE AND RITZ TECHNIQUE

(g) Hartmann number, M ≈ 100

Pipe outer-to-inner radii ratio, R	Pipe wall to fluid conductivity ratio, γ					
	0	0.1	0.5	1.0	1.5	2.0
	Average velocity, V_m/P_o					
1.00	8.15×10^{-3}	---	---	---	---	---
1.05	---	5.78×10^{-3}	2.73×10^{-3}	1.68×10^{-3}	1.23×10^{-3}	9.81×10^{-4}
1.15	---	3.80	1.28	7.40×10^{-4}	5.39×10^{-4}	4.34
1.25	---	2.92	8.93×10^{-4}	5.18	3.83	3.14
1.35	---	2.43	7.13	4.19	3.15	2.62
	Induced potential, W_{AD}/P_o					
1.00	1.51×10^{-2}	---	---	---	---	---
1.05	---	1.08×10^{-2}	5.12×10^{-3}	3.11×10^{-3}	2.24×10^{-3}	1.75×10^{-3}
1.15	---	7.08×10^{-3}	2.33	1.27	8.74×10^{-4}	6.66×10^{-4}
1.25	---	5.38	1.55	8.20×10^{-4}	5.58	4.23
1.35	---	4.40	1.18	6.15	4.17	3.15
	Sensitivity, S					
1.00	0.925	-----	-----	-----	-----	-----
1.05	---	0.932	0.936	0.926	0.910	0.893
1.15	---	.932	.906	.857	.811	.768
1.25	---	.921	.866	.792	.728	.673
1.35	---	.904	.825	.735	.661	.601
	Distortion factor, F_D					
1.00	0.925	-----	-----	-----	-----	-----
1.05	---	0.937	0.960	0.972	0.978	0.982
1.15	---	.954	.979	.986	.989	.991
1.25	---	.965	.985	.990	.992	.993
1.35	---	.972	.989	.992	.994	.995

TABLE III. - Continued. RESULTS FROM VARIATIONAL PRINCIPLE AND RITZ TECHNIQUE

(h) Hartmann number, M = 200

Pipe outer-to-inner radii ratio, R	Pipe wall to fluid conductivity ratio, γ					
	0	0.1	0.5	1.0	1.5	2.0
	Average velocity, V_m/P_o					
1.00	4.15×10^{-3}	---	---	---	---	---
1.05	---	2.27×10^{-3}	8.29×10^{-4}	4.72×10^{-4}	3.35×10^{-4}	2.62×10^{-4}
1.15	---	1.25	3.50	1.95	1.40	1.12
1.25	---	8.99×10^{-4}	2.37	1.34	9.83×10^{-5}	8.02×10^{-5}
1.35	---	7.21	1.87	1.08	8.05	6.67
	Induced potential, W_{AD}/P_o					
1.00	7.67×10^{-3}	---	---	---	---	---
1.05	---	4.26×10^{-3}	1.57×10^{-3}	8.84×10^{-4}	6.16×10^{-4}	4.72×10^{-4}
1.15	---	2.36	6.41×10^{-4}	3.36	2.28	1.72
1.25	---	1.67	4.14	2.13	1.44	1.08
1.35	---	1.31	3.10	1.59	1.07	8.04×10^{-5}
	Sensitivity, S					
1.00	0.924	-----	-----	-----	-----	-----
1.05	---	0.939	0.948	0.936	0.919	0.900
1.15	---	.942	.914	.862	.814	.771
1.25	---	.930	.872	.795	.730	.675
1.35	---	.912	.829	.737	.663	.602
	Distortion factor, F_D					
1.00	0.924	-----	-----	-----	-----	-----
1.05	---	0.945	0.972	0.983	0.987	0.989
1.15	---	.964	.987	.992	.993	.994
1.25	---	.975	.992	.994	.995	.996
1.35	---	.981	.993	.995	.996	.997

TABLE III. - Continued. RESULTS FROM VARIATIONAL PRINCIPLE AND RITZ TECHNIQUE

(i) Hartmann number, M = 500

Pipe outer-to-inner radii ratio, R	Pipe wall to fluid conductivity ratio, γ					
	0	0.1	0.5	1.0	1.5	2.0
	Average velocity, V_m/P_o					
1.00	1.68×10^{-3}	---	---	---	---	---
1.05	---	5.45×10^{-4}	1.52×10^{-4}	8.15×10^{-5}	5.66×10^{-5}	4.38×10^{-5}
1.15	---	2.46	5.93×10^{-5}	3.21	2.29	1.82
1.25	---	1.66	3.94	2.19	1.60	1.30
1.35	---	1.30	3.08	1.75	1.30	1.08
	Induced potential, W_{AD}/P_o					
1.00	3.10×10^{-3}	---	---	---	---	---
1.05	---	1.04×10^{-3}	2.93×10^{-4}	1.54×10^{-4}	1.05×10^{-4}	7.93×10^{-5}
1.15	---	4.71×10^{-4}	1.09	5.57×10^{-5}	3.74×10^{-5}	2.81
1.25	---	3.13	6.91×10^{-5}	3.50	2.34	1.76
1.35	---	2.39	5.13	2.59	1.73	1.30
	Sensitivity, S					
1.00	0.924	-----	-----	-----	-----	-----
1.05	---	0.952	0.965	0.946	0.926	0.906
1.15	---	.955	.921	.866	.817	.773
1.25	---	.941	.876	.798	.732	.677
1.35	---	.924	.833	.739	.664	.603
	Distortion factor, F_D					
1.00	0.924	-----	-----	-----	-----	-----
1.05	---	0.958	0.989	0.994	0.995	0.995
1.15	---	.978	.995	.996	.997	.997
1.25	---	.986	.996	.997	.998	.998
1.35	---	.994	.997	.998	.998	.998

TABLE III. - Concluded. RESULTS FROM VARIATIONAL PRINCIPLE AND RITZ TECHNIQUE

(j) Hartmann number, M = 1000

Pipe outer-to-inner radii ratio, R	Pipe wall to fluid conductivity ratio, γ					
	0	0.1	0.5	1.0	1.5	2.0
	Average velocity, $V_m P_o$					
1.00	8.43×10^{-4}	---	---	---	---	---
1.05	---	1.64×10^{-4}	3.99×10^{-5}	2.09×10^{-5}	1.44×10^{-5}	1.11×10^{-5}
1.15	---	6.67×10^{-5}	1.51	8.12×10^{-6}	5.76×10^{-6}	4.57×10^{-6}
1.25	---	4.39	9.98×10^{-6}	5.52	4.02	3.26
1.35	---	3.38	7.78	4.41	3.27	2.71
	Induced potential, $W_{AD} P_o$					
1.00	1.56×10^{-3}	---	---	---	---	---
1.05	---	3.15×10^{-4}	7.75×10^{-5}	3.98×10^{-5}	2.67×10^{-5}	2.01×10^{-5}
1.15	---	1.29	2.79	1.41	9.42×10^{-6}	7.08×10^{-6}
1.25	---	8.33×10^{-5}	1.75	8.81×10^{-6}	5.89	4.42
1.35	---	6.27	1.30	6.52	4.35	3.27
	Sensitivity, S					
1.00	0.924	-----	-----	-----	-----	-----
1.05	---	0.963	0.972	0.949	0.928	0.908
1.15	---	.963	.924	.868	.818	.774
1.25	---	.948	.877	.799	.733	.677
1.35	---	.928	.834	.740	.665	.604
	Distortion factor, F_D					
1.00	0.924	-----	-----	-----	-----	-----
1.05	---	0.969	0.997	0.997	0.997	0.997
1.15	---	.986	.997	.998	.998	.998
1.25	---	.993	.998	.998	.999	.999
1.35	---	.998	.998	.999	.999	.999

"The aeronautical and space activities of the United States shall be conducted so as to contribute . . . to the expansion of human knowledge of phenomena in the atmosphere and space. The Administration shall provide for the widest practicable and appropriate dissemination of information concerning its activities and the results thereof."

—NATIONAL AERONAUTICS AND SPACE ACT OF 1958

NASA SCIENTIFIC AND TECHNICAL PUBLICATIONS

TECHNICAL REPORTS: Scientific and technical information considered important, complete, and a lasting contribution to existing knowledge.

TECHNICAL NOTES: Information less broad in scope but nevertheless of importance as a contribution to existing knowledge.

TECHNICAL MEMORANDUMS: Information receiving limited distribution because of preliminary data, security classification, or other reasons.

CONTRACTOR REPORTS: Scientific and technical information generated under a NASA contract or grant and considered an important contribution to existing knowledge.

TECHNICAL TRANSLATIONS: Information published in a foreign language considered to merit NASA distribution in English.

SPECIAL PUBLICATIONS: Information derived from or of value to NASA activities. Publications include conference proceedings, monographs, data compilations, handbooks, sourcebooks, and special bibliographies.

TECHNOLOGY UTILIZATION PUBLICATIONS: Information on technology used by NASA that may be of particular interest in commercial and other non-aerospace applications. Publications include Tech Briefs, Technology Utilization Reports and Technology Surveys.

Details on the availability of these publications may be obtained from:

SCIENTIFIC AND TECHNICAL INFORMATION OFFICE

NATIONAL AERONAUTICS AND SPACE ADMINISTRATION

Washington, D.C. 20546